ab-initio STUDIES OF MAGNESIUM HYDRIDE AND LITHIUM HYDRIDE FOR HYDROGEN STORAGE APPLICATIONS: A DENSITY FUNCTIONAL THEORY STUDY

BY

MAGERO DENIS

SC/PGC/018/10

A THESIS SUBMITTED IN PARTIAL FULFILMENT OF THE REQUIREMENTS FOR THE DEGREE OF MASTER OF SCIENCE IN CHEMISTRY OF UNIVERSITY OF ELDORET.

2013

DECLARATION

This thesis is my original work and has not been presented for a degree in any other University. No part of this thesis may be reproduced without the prior written permission of the author and/or University of Eldoret.

Magero Denis

Signature: ..... Date: .....

SC/PGC/018/10

Approval by Supervisors

This thesis has been submitted for examination with our approval as University of Eldoret supervisors.

Signature: ..... Date: .....

Professor Lusweti Kituyi,

Department of Chemistry and Biochemistry, University of Eldoret, Eldoret, Kenya

Signature: ..... Date: .....

Dr. Nicholas Makau,

Department of Physics, University of Eldoret, Eldoret, Kenya

Signature: ..... Date: .....

Professor George Amolo,

Department of Physics, University of Eldoret, Eldoret, Kenya

Signature: ..... Date: .....

Dr. Muhavini C. Wawire,

Department of Natural Science (Chemistry), The Catholic University of Eastern Africa, Nairobi, Kenya

DEDICATION

To my beloved family: Benedict Magero, Judith Magero, Pius Magero and Laura Manoti for your unconditional love and support.

ABSTRACT

Due to the imminent exhaustion of fossil fuels, related pollution and high cost involved in conventional sources of energy, a search for renewable, environmentally friendly, cheaper and more efficient energy sources has been on the increase. Hydrogen as a fuel is seen as one of the promising energy technologies alternative to fossil fuels. Metal hydrides have been suggested as potential candidates for the bulk storage of hydrogen. However, the limitations of hydrogen storage in metal hydrides include high thermodynamic stability, high desorption temperature and low plateau pressure at ambient temperature. In this study, *ab-initio* calculations were performed on two metal hydrides that are promising candidates for hydrogen storage applications, that is, magnesium hydride (MgH_2) and lithium hydride (LiH). Density functional theory (DFT) calculations using the Quantum Espresso code was employed to study the bulk, structural, electronic and thermodynamic properties of the two metal hydrides. The study was based on the bulk rutile type MgH_2 and the rock salt type LiH structure. Calculated lattice parameter of MgH_2 was $a = b = 4.54$ Å and $c = 3.019$ Å showing a deviation of +0.8% for both dimensions from the experimental values of $a = 4.515$ Å and $c = 3.01$ Å. LiH had a calculated lattice parameter of $a = b = c = 3.93$ Å compared to an experimental value of $a = b = c = 4.083$ Å indicating a deviation of -3.7%. Bulk modulus was calculated as 56.85 GPa and 39.9 GPa for MgH_2 and LiH, respectively. The electronic band gap for MgH_2 was calculated to be 3.65 eV which was an indirect one occurring from Z to A. That of LiH was a direct electronic band gap of 3.0 eV. Projected Density of States for both LiH and MgH_2 indicated the presence of some covalent bonds. Cohesive energy for MgH_2 was calculated as 13.6 eV per unit cell while the calculated formation energy was -78.20 kJ/mol.H_2 and -178.137 kJ/mol.H_2 for MgH_2 and LiH respectively. Entropy, specific heat and internal energy for both MgH_2 and LiH increase with temperature. The vibrational energy for both MgH_2 and LiH decrease with temperature. Results from all the plots indicate that the calculated results are close to experimental values with a deviation of 2% from the experimental values. The properties obtained in this study for the two materials are key in determining their suitability for hydrogen storage applications, and all suggest that both LiH and MgH_2 can be used for hydrogen storage. There is need to study more on the surface properties of the two metal hydrides since hydrogen desorbs from bulk to surface.

TABLE OF CONTENTS

LIST OF FIGURES

LIST OF TABLES

LIST OF SYMBOLS AND ABBREVIATIONS OF ACRONYMS

The following are the symbols and acronyms used in this thesis.

ICE	Internal combustion engine
PEM	Proton exchange membrane
MOF's	Metal organic frameworks
QHA	Quasiharmonic approximation
T_o	Kinetic energy of ions
V_{ion}	Ion-ion Potential energy
ψ	Many electron wave function
V_{ext}	External potential
$F[n(r)]$	Functional of density
E_{xc}	Exchange and correlation energy of interacting system
$\bigtriangledown$	Gradient operator/ Laplacian operator
$\approx$	Approximately
E_{cut}	Plane wave cutoff energy
Å	Angstrom unit
B_0	Bulk modulus
E_{coh}	Cohesive energy
$\hat{H}$	Hamiltonian operator
G	Reciprocal lattice vectors
a_0	Lattice constant
E	Internal Energy

EoS	equation of state
Q.E	Quantum ESPRESSO
F	Helmholtz free energy
DFT	Density functional theory
LDA	Local density approximation
GGA	Generalized gradient approximation
IBZ	Irreducible brillouin zone
PBE	Perdew Burke Ernzerhof
PW	Plane Wave
pwscf	plane wave self consistent field
scf	self consistent field
USPP	Ultra-soft pseudopotential
GRACE	Graphing Advanced Computing and Exploration of data
XCrysDen	X-window Crystalline Structure and densities

ACKOWLEDGEMENTS

I would like to thank my supervisors, Professor Lusweti Kituyi, Dr. Nicholas Makau, Professor George Amolo and Dr. Cleophas Muhavini. Thank you very much for giving me this great opportunity to get into the exciting world of computational modelling. It has opened up for me great opportunities in life that I had never imagined before. I deeply appreciate your priceless guidance, support and motivation to share every bit of your knowledge and ideas until the very end. Thanks for giving me the opportunity to learn with you and for believing in me. I salute all my graduate lecturers who taught me during course work.

I also wish to appreciate the developers of Quantum ESPRESSO code that I used in all calculations in this work and the International Centre of Theoretical Physics (ICTP) is acknowledged for organizing schools and workshops that were of great importance for this work. I would like to acknowledge Professor Ryo Maezono of the Japanese Advanced Institute for Science and Technology (JAIST) and the Centre for High Performance Computing (CHPC) in South Africa, for providing their computing facilities for the numerical calculations performed in this study. Thanks to Professor Mark Casida of the Grenoble Institute in France for taking your time to offer lectures in the area of Quantum Chemistry.

I am deeply indebted to my dearest friends in the Computational Material Science Group of University of Eldoret. I would like to express my deep gratitude to my dear friend Rodah Soy Cheruto for always being there and for her support.

This work was supported by the National Commission for Science, Technology and Innovation (NACOSTI), Kenya grant number NCST/ST&I/RCD/4^{th} CALL M.Sc/149.

CHAPTER ONE

INTRODUCTION

1.1 Hydrogen as a Fuel

Environmental degradation due to the use of fossil fuels and other traditional sources of energy such as nuclear energy has led to an urgent need for alternative cleaner sources of energy. Limited energy resources and growing pollution associated with conventional process of energy production and use have stimulated the search for cleaner, cheaper and more efficient energy technologies. One promising technology involves hydrogen as a fuel (Schlapbach and Zuttel, 2001; Sakintuna *et al.,* 2007; Varin *et al.,* 2008). Hydrogen in this respect is an environmentally benign, safe and attractive medium; being among the most abundant element in the universe, with a high energy density per unit weight (chemical energy of hydrogen; 142 MJ/kg is at least three times larger than that of other chemical fuels, that is, fuels that release energy by reacting with substances around them, most notably the process of oxidation) and water as the major by-product of its combustion. Hydrogen is an attractive source of chemical potential energy as it is made up of only one proton and one electron, giving it the best ratio of valence electrons available for reaction per unit mass.

The chemical potential of hydrogen can either be harnessed by combustion in an internal combustion engine (ICE) to produce mechanical power, in the same way that petroleum is currently used, or electrochemically using a fuel cell to produce electrical power. Hydrogen can be obtained from raw materials such as coal, water, among others. This can be achieved by using various renewable sources of energy including solar energy, wind power, hydroelectric, biomass and geothermal (Schlapbach and Zuttel, 2001). The greatest technical barrier to harnessing hydrogen as a fuel is the storage of hydrogen in a compact and lightweight form (Wu *et al.,* 2009). A great deal of effort has been made on new hydrogen-storage systems, including metal, chemical or complex hydrides and carbon nano structures. Solid-state hy-

drogen fuel storage by either absorption in the interstices of metals and metallic alloys or adsorption on high surface area materials such as activated carbons has gained the attention for possible future hydrogen applications. The reason for this is that storing hydrogen in gas and liquid state is more energy intensive and costly than the solid-state hydrogen storage. Metal hydrides therefore represent potential candidates for solid state hydrogen storage due to their high hydrogen capacity by weight (7.6 wt %), abundance in the earth's crust and low cost and non-toxic nature (Schlapbach and Zuttel, 2001; Sakintuna *et al.,* 2007; Varin *et al.,* 2008; Wu *et al.,* 2009; Novakovi *et al.,* 2007). Figure 1.1 shows the energy content per unit mass of different sources, where the superiority of hydrogen is clearly demonstrated.

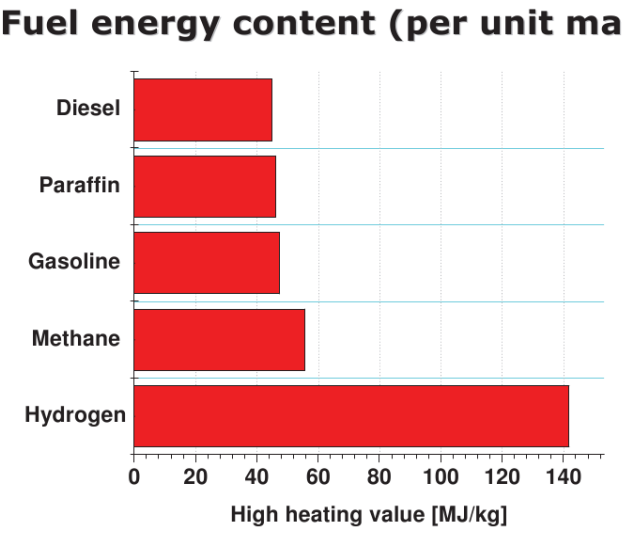

Figure 1.1: A comparison of fuel energy content per unit mass in (MJ/kg) for different fuels (Ball and Wietschel, 2009).

1.2 Hydrogen Fuel Cells

Fuel cells are electrochemical energy cells that produce electricity from fuel sources. The chemical potential of a reaction is used to drive an electrical current around a circuit. Fuel cells are classified into many types depending on the electrolyte used: molten carbonate, solid oxide, alkaline, phosphoric acid, and polymer membrane electrolytes are the most common. The use of fuel cells with hydrogen is seen as the ultimate step in clean energy usage (Edwards *et al.,* 2008).

Polymer electrolyte membrane fuel cells, also known as proton exchange membrane (PEM) fuel cells are electrochemical cells that produce electricity from a fuel source, usually molecular hydrogen gas. They operate with high efficiency at temperatures around 338K (Barbir and Gomez, 1997), making them particularly attractive for mobile applications. Hydrogen gas is supplied at the anode, where a catalyst (typically platinum) splits the hydrogen into its component protons and electrons. The polymer membrane allows only the protons to permeate through it, forcing the electrons to travel along an external circuit providing electrical power. Air containing oxygen is allowed to flow past the cathode, whereby the electrons from the circuit recombine with the protons and oxygen at the cathode to form water. The water may be stored and disposed off later or it can be used for cooling purposes. In practice, many PEM fuel cells are used in combination to produce a fuel cell stack so that higher power densities can be achieved. Many automotive manufacturers have produced cars containing PEM fuel cells such as General Motors' Chevrolet Equinox Fuel Cell in 2009. PEM fuel cells can/may be however adversely affected by the presence of contaminants in the hydrogen supply (Cheng *et al.,* 2007).

1.3 Hydrogen Storage Methods

The storage of hydrogen involves the reduction in volume of hydrogen from its natural state as a diatomic gas, which occupies 11 m^3 kg^{-1} at standard temperature and pressure, to a more usable volumetric density. Increases in volumetric density can easily be achieved by various methods such as compression or liquefaction but this is always at the expense of gravimetric density. An ideal hydrogen storage system is a compromise between increasing the volumetric capacity of the system while maintaining a usable gravimetric hydrogen capacity. This can be done in a number of ways; the storage of hydrogen as molecular or atomic/ionic hydrogen. A hydrogen storage system for molecular hydrogen increases the volumetric density by physical compression of the gas, by liquefaction or by adsorption on surfaces.

Atomic hydrogen can be stored by reaction of hydrogen gas to form metal hydrides or complex hydrides. The reversible storage of hydrogen for both stationary and mobile applications could be in several forms; such as gaseous, liquid, physisorption in carbon nanotubes, metal and complex hydrides (Zuttel, 2003).

1.3.1 Pressurized Gas

High-pressure gas tanks are currently the most widely used and understood technology. The commercial tanks made from steel can operate with pressures of up to 200 bars (Schlapbach and Zuttel, 2001), whereas, composite cylinders developed so far can stand pressures of up to 800 bars and contain 36 kg hydrogen per m^3 volume. The gravimetric hydrogen densities are markedly reduced due to the necessity of using thick walled cylinders that can withstand such high pressures. The energetic cost of pressurizing hydrogen is also substantial. Handling of gas at such high pressures introduces a series of challenges, as the gas pressure leaving the pressure vessel must be stepped down so that it can be used. There are also safety concerns with storing gas at very high pressures. Hybrid pressure vessels which combine metal hydrides with a high pressure tank have been proposed (Takeichi *et al.,* 2003).

1.3.2 Physisorption

Physisorption is the process of attracting and holding a molecule to a surface through van der Waals interactions. These weak, intermolecular forces are caused by electrostatic interactions and result from both permanent and induced poles in the electronic field of an atom or molecule. Like all gases, hydrogen will adsorb onto solid surfaces via attractive Van der Waals-type interactions. The energy of these interactions is typically very low, being in the range of 2 - 30 kJ mol^{-1} H_2 (Zuttel, 2004), and thermal energy at room temperature is enough to desorb the majority of hydrogen from the surface. Low temperatures are used to maximize this interaction. The strongest binding of hydrogen will occur when the hydrogen is bound in a single layer on the surface; subsequent layers will be less tightly bound. Materials

for hydrogen storage via physisorption are typically very high surface area solids such as zeolites (Langmi *et al.,* 2005), high surface area carbon (Yang *et al.,* 2007), metal-organic frameworks (MOFs) (Lin *et al.,* 2006) or polymers of intrinsic microporosity (PIMs) (Budd *et al.,* 2007). Materials such as zeolites and MOFs have the potential to increase the strength of the hydrogen binding by the inclusion of metal ions within the structures. Purely surface interactions can give rise to hydrogen capacities of approximately 1.6 wt% (Zuttel, 2004; Langmi *et al.,* 2005), whereas gravimetric capacities of 6.7 wt% have been reported for MOFs where binding to metal centres is believed to increase the hydrogen capacity (Walker, 2008).

1.3.3 Cryogenic Liquid

Liquid form of hydrogen storage has been extensively used in space technology for several years (Sherif *et al.,* 1997). Storing hydrogen as liquid takes less space than storage as pressurized gas. The volumetric density of liquid hydrogen is 70 kg per m^3, which is almost twice that of the pressurized gas at 800 bars. Once liquefied, it can be maintained as a liquid in thermally insulated containers. However, liquid hydrogen has an extremely low boiling temperature of 20 K, which is actually the second lowest boiling temperature in nature after helium; consequently, it requires very sophisticated insulation techniques to keep hydrogen in liquid form. Taking into account the high energetic cost of hydrogen liquefaction, about 15.2 kWh/kg (Zuttel, 2004), together with the difficulties in maintenance, one can conclude that the although liquid hydrogen is usable, it is not cost effective to use it.

1.3.4 Metal Hydrides

Metal hydrides are important energy storage materials. They have been classified into three main categories: (i) classical metal hydrides, (ii) chemical hydrides, and (iii) light metal complex hydrides (Walker, 2008). Hydrogen forms metal hydrides with some metals and alloys leading to solid-state storage under moderate temperature and pressure. There are two possible ways of hydriding a metal, that is, direct

dissociative chemisorption and electrochemical splitting of water (Sakintuna *et al.,* 2007). These reactions are:

$$M_{(s)} + \frac{x}{2} H_{2(g)} \rightleftharpoons MH_{x(s)}, \tag{1.1}$$

$$M_{(s)} + \frac{x}{2} H_2O_{(l)} + \frac{x}{2} e^- \rightleftharpoons MH_{x(s)} + \frac{x}{2} OH^-_{(aq)}. \tag{1.2}$$

Where M is the metal.

Metal hydride formation involves dissociative chemisorption of H_2 on to a metal surface and then H atom diffusion starts into the crystal lattice. The formation of metal hydrides is typically exothermic and hydrogen desorption from the hydrides can be achieved endothermally under appropriate thermodynamic conditions (Sakintuna *et al.,* 2007). Metal hydrides are composed of metal atoms that constitute a host lattice and hydrogen atoms. The metal and hydrogen atoms usually form two different kinds of hydrides; α phase at which only some hydrogen is absorbed and β-phase at which the hydride is fully formed. Hydrogen storage in metal hydrides depends on different factors and consists of several mechanistic steps. Metal hydrides differ in their ability to dissociate hydrogen, and this ability is dependent on surface structure, morphology and purity (David, 2005).

An optimum hydrogen-storage material is to have the following properties;

• High hydrogen capacity per unit mass and unit volume which determines the amount of available energy,

• Low dissociation temperature, moderate dissociation pressure, low heat of formation in order to minimize the energy necessary for hydrogen release,

• Low heat dissipation during the exothermic hydride formation, reversibility, limited energy loss during charge and discharge of hydrogen,

• Fast kinetics, that is, hydrogenation and dehydrogenation,

• High stability against oxygen and moisture for long cycle life,

• Cyclibility,

• Low cost of recycling and charging infrastructures and high safety (Sakintuna

et al., 2007).

The light metals such as Li, Be, Na, Mg and Al form a large variety of metal hydrogen compounds. They are especially interesting due to their light weight and the number of hydrogen atoms per metal atom. Heavier ones may enter the multiple component system only as a low abundant additive, most likely for alteration of properties or as a catalyst. The hydrides of the first and especially the second group (Novakovi *et al.,* 2007) of the periodic table; which includes Li and Mg have been suggested as potential candidates for the bulk storage of hydrogen. The main advantage of these metal hydrides with respect to any other storage medium has been the lightweight, low cost and high hydrogen density (David, 2005; Principi *et al.,* 2009). Metal hydrides have higher hydrogen-storage density (6.5 H atoms/cm^3 for MgH_2) than hydrogen gas (0.99 H atoms/cm^3) or liquid hydrogen (4.2 H atoms/cm^3) (Lide, 2012).

Extensive research has been recently reported on the metal hydrides on modifying and optimizing them for hydrogen-storage. This includes: improving adsorption/desorption properties based on hydrogen storage capacity, kinetics, thermal properties, toxicity, cycling behaviour and cost, hence finding optimum solid hydrogen-storage system (Sakintuna *et al.,* 2007). The large-scale utilization of hydrogen as a fuel crucially depends on the development of compact storage materials with a high mass content of hydrogen (Schuth *et al.,* 2004). However, high thermodynamic stability, high desorption temperature and low plateau pressure at ambient temperature limit metal hydride practical applications (Schlapbach and Zuttel, 2001; Sakintuna *et al.,* 2007; Varin *et al.,* 2008; Wu *et al.,* 2009; Novakovi *et al.,* 2007), as noted earlier.

A deeper understanding of the bulk and electronic structure and related mechanical properties of metal hydrides is therefore important for their applications as storage compounds. *Ab-initio* calculations are very useful for understanding the chemical and physical properties of various materials. The calculations also give a principal direction for estimation and prediction of the un-measured yet important

characteristics of studied compounds (Brika and Kityk, 2011). In Density Functional Theory calculations, the crystal structure with the lowest energy has to be searched for each compound, and the cell parameters and the atomic positions have to be optimized.

This work presents *ab-initio* calculations of the most important properties of the two metal hydrides under investigation; these are MgH_2 and LiH. MgH_2 is one of the most important metal hydrides for reversible storage of hydrogen because of its light weight and cost as well as the high theoretical hydrogen storage capacity (MgH_2 has approximately 7.6 % of hydrogen). LiH on the other hand is the simplest in terms of its molecular structure.

1.4 Problem Statement

Exhaustion of fossil fuel reserves, environmental pollution, increasing demands and high prices for oil and the need for energy security have become the most urgent drivers for the search for alternative energy sources. Therefore, hydrogen fuel represents an alternative energy source due to its high energy density and zero or low carbon emission properties. However, one of the major obstacles to utilizing hydrogen as an energy carrier is storage. Storing hydrogen in gaseous and liquidous states is more energy intensive and costly than the solid-state hydrogen storage (metal hydrides), which is therefore of great interest for this purpose. This study therefore investigates the properties of MgH_2 and LiH as the two metal hydrides that have been predicted to have a high potential for use in solid-state hydrogen storage. The large-scale utilization of hydrogen as a fuel crucially depends on the development of compact storage materials with a high mass content of hydrogen. However, high thermodynamic stability, high desorption temperature and low plateau pressure at ambient temperature limits the practical applications of metal hydrides. This study will theoretically investigate the mechanical, electronic and thermodynamic properties of the two metal hydrides in detail, which are all of paramount importance for their applications as hydrogen storage compounds.

1.5 Significance of the Study

The importance of hydrogen as an alternative energy source is based on the fact that it is carbon neutral since burning hydrogen produces only water as the by-product unlike fossil fuels which produce also CO_2. In addition, renewable sources that can be used to produce hydrogen are domestically available at low cost and abundant in nature. Metal hydrides are major candidates for hydrogen storage because of their relative ease of hydrogen production. MgH_2 is particularly of great interest because it can store up to 7.6 % of hydrogen by weight, which is a large enough quantity for hydrogen storage applications, if all the hydrogen in the material can be made available when required. Other than being a suitable candidate for hydrogen storage, LiH also has the advantage of being the simplest in terms of its simple molecular structure.

1.6 Objectives

1.6.1 General Objective

To study the properties magnesium and lithium hydrides for hydrogen storage applications.

1.6.2 Specific Objectives

1. To determine the equilibrium structural properties of magnesium and lithium hydrides by *ab-initio* methods.

2. To determine the mechanical properties of magnesium and lithium hydrides by *ab-initio* methods.

3. To determine the electronic properties of magnesium and lithium hydrides by *ab-initio* methods.

4. To determine the thermodynamic properties of magnesium and lithium hydrides using the quasi harmonic approximation (QHA).

CHAPTER TWO

LITERATURE REVIEW

2.1 Magnesium Hydride

Magnesium Hydride has been suggested as a potential hydrogen storage material (Sakintuna *et al.,* 2007). This section reviews some of the work that has been done towards achieving the use of MgH_2 as a hydrogen storage material.

2.1.1 Magnesium Hydride for Hydrogen Storage

MgH_2 has a great potential for on-board hydrogen storage application due its high hydrogen content 7.6 wt. % and volumetric density which is about twice that of liquid hydrogen. Apart from that, Mg is also easily accessible and is a low cost material. The Mg based hydrides possess good-quality functional properties, such as heat-resistance, vibration absorbing, reversibility and recyclability (Sakintuna *et al.,* 2007). MgH_2 has the highest energy density (9 MJ/kg Mg) of all reversible hydrides applicable for hydrogen storage.

Due to its high theoretical gravimetric capacity of 7.6 wt. %, low density, reversibility ($MgH_2 \leftrightarrow Mg$) low cost, and abundance in the earth's crust, MgH_2 has been the subject of extensive studies (Sakintuna *et al.,* 2007). This compound differs from other metal hydrides according to the type of metal-hydrogen bonds and its crystal structure as well as properties and it is similar to ionic hydrides of alkali and alkaline earth metals. The equilibrium modification of MgH_2 under normal conditions, α-MgH_2 has a tetragonal crystal structure of the rutile type (Bortz *et al.,* 1999), while under high pressure α-MgH_2 undergoes polymorphic transformations to form two modifications: γ–MgH_2 and β – MgH_2, with an orthorhombic structure and a hexagonal structure, respectively (Gennari *et al.,* 2002).

2.1.2 Properties of Mg/MgH_2

MgH_2 is appropriate for hydrogen storage because it meets some of the important hydrogen storage criteria. These include MgH_2 having the highest energy density (9 MJ/kg Mg) of all reversible hydrides used for hydrogen storage. MgH_2 has a high H_2 capacity of 7.7 wt. % furthermore Mg is abundantly available at low cost with good reversibility (Zhu *et al.,* 2006).

2.1.3 Factors Limiting MgH_2 for Practical Application

MgH_2 has the desired properties required for practical hydrogen storage applications but still it cannot be used on board, that is, it cannot be used practically. The major disadvantages of MgH_2 as a hydrogen storage material is the high temperature of hydrogen discharge, slow desorption kinetics and a high reactivity towards air and oxygen (Zaluska *et al.,* 1999). The high thermodynamic stability of the Mg hydride prevents dehydrogenation under moderate conditions. This is because of the slow cleavage of dihydrogen to atomic hydrogen and the low diffusion rate in MgH_2.

There are several factors that significantly reduce the rate of hydrogenation. One of them is the oxidation of magnesium surface and/or formation of magnesium hydroxide. Magnesium oxide forms quite easily on a Mg surface that is exposed to air. Usually oxide layers on the metal surface are not transparent to hydrogen molecules and hence MgO layer prevents hydrogen molecules from penetrating into the material (Manchester and Khatamian, 2008) to initiate hydrogen absorption. For this to happen, the oxide layer should be broken down by an activation process.

Low dissociation rate of hydrogen molecules on the metal surface is another reason for the slow hydrogenation rate of magnesium. A clean surface of pure magnesium needs a very high energy for dissociation (Zaluska *et al.,* 1999). Diffusion of dissociated hydrogen atoms within metal hydride is very difficult. The growth rate of MgH_2 phase depends on the hydrogen pressure since, as the pressure increases, the thermodynamic driving force for the reaction increases.

2.1.4 Ways of Improving Sorption Properties of Magnesium Hydride

As it is, MgH_2 is not considered to be useful for hydrogen storage purposes because of the high decomposition temperature and the slow kinetics of hydrogen intake. A number of attempts have been made to modify this material to improve its properties. Some of the efforts include ball milling, alloying, catalysis and intermetallic compounds.

2.1.4.1 Ball Milling

Ball milling introduces clusters of defects, which may assist diffusion of hydrogen. It also lowers the barrier for nucleation of MgH_2, produces mechanical deformation and metastable phases, and modifies surfaces. The main effects of ball-milling are increased surface area, formation of micro/nanostructures and creation of defects on the surface and in the interior of the material. The induced lattice defects may aid the diffusion of hydrogen in materials by providing many sites with low activation energy of diffusion.

The induced micro strain assists diffusion by reducing the hysteresis of hydrogen absorption and desorption (Guoxian *et al.,* 1995). These effects generally promote the solid–gas reaction (Kokalj, 2003; Noritake *et al.,* 2003). Depending on the ball milling conditions, the onset temperature of MgH_2 desorption can be decreased by as large as 373 K. Decrease in crystal grain size causes the desorption energy to decrease drastically, reducing the desorption temperature to up to 373 K (Zaluska *et al.,* 1999). Milling under hydrogen atmosphere provides an easy way to diffuse hydrogen into the material.

Liang *et al.,* (1998) investigated the structural difference between milled and unmilled MgH_2. The specific surface area decreased by milling 10 fold. Faster hydrogen desorption kinetics, reduction in activation energy and enhanced kinetics was observed for the milled MgH_2 compared to the unmilled one as 120 and 156 kJ/mol for the milled and unmilled powders, respectively.

Wagemans *et al.,* (2005) investigated the quantum chemical perspective of MgH_2.

Small MgH_2 clusters were found to have much lower desorption energy than bulk MgH_2, hence enabling hydrogen desorption at lower temperatures. The hydrogen desorption energy decreases significantly when the crystal grain size becomes smaller than 1.3 nm. A MgH_2 crystallite with a size of 0.9 nm corresponds to a desorption temperature of only 473 K. Particles with nanocrystalline structure with grain size of 10 nm or less have been found to increase the density of grain boundaries, thereby resulting in easier activation (Hong *et al.,* 2000).

Chen and Williams, (1995) studied the formation of metal hydrides under H_2 atmosphere. Their results indicated that pulverization and deformation processes occurring during high-energy ball-milling play a major role in the hydriding reaction. It is thus concluded that ball-milling is a simple and inexpensive method of producing high hydrogen content metal hydrides.

2.1.4.2 Alloying with Other Transition Metal and their Oxides

Alloying has been shown to reduce the desorption temperature and to remove other thermodynamic constraints. It has been found that the hydrogenation properties of Mg, such as hydrogenation/dehydrogenation temperature and hydrogenation rate, can be more or less improved by forming composite structures.

Zhu *et al.,* (2006), reported that the hydrogen sorption properties of Mg and Mg–Ni-based alloys can significantly be improved by forming composites having proper micro structural features. The nanocrystalline Mg_2Ni intermetallic compound formed by mechanical alloying of Mg and Mg_2Ni can absorb hydrogen rapidly without activation. The Mg + Mg_2Ni composites need activation, but once activated, they absorb hydrogen more rapidly than Mg_2Ni at low temperature of 423 K under 12 bar with high capacity of 4.2 wt%. Nanoparticles of Mg_2Ni lead to superior hydrogenation behaviour including easy activation and hydrogen uptake in the first cycle itself compared to the conventional crystal phase. Nanocrystalline Mg_2Ni with Pd has been found to exhibit even much faster absorption kinetics at 473 K than the ball-milled samples (Liang *et al.,* 1998).

2.1.4.3 Catalysis

Catalysis is a critical factor in the improvement of hydrogen sorption kinetics in metal hydride systems that enable fast and effective dissociation of hydrogen molecules (Zaluska *et al.,* 1999). The rate of absorption is controlled by the following factors: the rate of hydrogen dissociation at the surface, the capability of hydrogen to penetrate from the surface which is typically covered by an oxide layer into metal, the rate of hydrogen diffusion into the bulk metal and through the hydride already formed.

Palladium (Pd) is considered a good catalyst for hydrogen dissociation reaction. Pd enhances the hydriding properties through nanoparticles located on the magnesium surface. The reactivity of palladium after exposure to oxygen is recovered during exposure to hydrogen because of the easy decomposition of palladium oxide. The presence of Pd as a catalyst in nanocrystalline Mg_2Ni, $LaNi_5$ and FeTi systems, enhances the absorption rates of hydrogen even at lower temperatures and maintains less sensitivity to air exposures (Zaluski *et al.,* 1995).

Hydrogen molecules have a strong affinity for nickel and readily dissociate and adsorb onto surface-layer nickel clusters (Bloch and Mintz, 1997). Through the addition of 1% of nickel to magnesium, Holtz and Imam (1999) achieved a 50% increase in hydrogen capacity, a decrease in the temperature for the onset of hydrogenation from 548 to 448 K, and a lowering of the dehydrogenation onset temperature from 623 to 548 K. In addition to Pd and Ni, Ge can be used for the catalysis of hydrogenation kinetics (Gennari *et al.,* 2001). The presence of Ge decreases the hydride decomposition temperature in a range from 323 to 423 K, depending on the catalyst amount. Vanadium also acts as a catalyst for the dissociation of hydrogen molecules. It was also reported using vanadium as a catalyst that hydrogen capacity can be increased by up to 5.8 wt% while the thermodynamic parameters of MgH_2 were not altered (Dehouche *et al.,* 2002).

Catalyst type and the amount of catalysts used have a significant effect on hydrogen absorption behaviour. Oelerich *et al.,* (2001), investigated different amounts

of oxides for catalysis but it was shown that only 0.2 mol% of the catalyst is sufficient to provide fast sorption kinetics. In the search for efficient and inexpensive catalysts for hydrogen sorption reactions, a new type of catalytic compounds was developed. These catalytic complexes demonstrated remarkable enhancement in sodium alanates and magnesium, as well as in hydrogen generation through hydrolysis (Zaluska and Zaluski, 2005).

2.1.4.4 Intermetallic Compounds

Among additives that can be used to improve hydrogen storage capacities, include metals like Ni, Pd or Ti which form hydrides, that can behave as "hydrogen pumps" and transition metals such as Fe, Co or Cr, which, favour the hydrogen molecule dissociation and the phase transformation of Mg matrix to MgH_2 (Huot *et al.,* 2001). In both cases the material performances depend, among other factors, on the optimization of the synthesis procedure and on the amount of catalyst since both parameters play a critical role to obtain the best dispersion in matrix and optimum sorption properties.

As far as the transition metals are concerned, Bobet *et al.,* (2000) reported that the addition of Co or Fe during reactive ball milling of Mg significantly increases the quantity of formed MgH_2, since the processing was able to induce reduction of Mg particle size and easy formation of hydride phase. They were able to show that a proper microstructure with short hydrogen diffusion distances improves the hydrogen sorption kinetics.

Moreover, excellent performances were also obtained by adding more than one catalyzing material like 1 wt. % Ni to 0.2 wt. % Pd. In this case, the combined effect of Pd and Ni induces fast nucleation sites for phase transformation during both absorption and desorption processes and even if nanocrystallinity of the powder is largely lost during heat treatments in H_2, the reaction kinetics remains excellent over more than 50 cycles (Montone *et al.,* 2007).

It has been found that inhomogeneous catalyst distribution results for a small

amount (2 or 5 wt. %) of catalyzing metal and for a low value of the milling intensity (Ball to Powder Ratio-BPR-1:1 or 3:1). In these cases, large volumes free from catalyst are observed, which results in a two-step dehydrogenation process and only a fraction of the total hydrogen is released at temperatures lower than that characteristic for pure milled MgH_2.

2.2 Lithium Hydride

2.2.1 Properties of Lithium Hydride

Natural lithium contains two stable isotopes ^{6}Li (7.59%) and ^{7}Li (92.41%), while on the other hand, hydrogen has three natural stable isotopes: hydrogen (99.985%), deuterium (0.015%) and tritium (0.00010 - 0.00015%) (Cheng *et al.,* 2007). Lithium hydride is a standard benchmark molecule in electronic structure because it is a small system, which exhibits features of more complicated molecules. Like the H_2 molecule, it is singly bonded with a closed-shell electron configuration in the ground state. On the other hand, its four electrons give rise to higher order correlation effects, which are not possible in H_2. LiH lacks the simplifying features, which originate from a symmetry inversion centre in homo-nuclear diatomic molecules, and this makes it a standard system for dipole moments and other properties (Lee *et al.,* 1997).

The lithium hydride isotopes (^{6}LiH, ^{6}LiD, ^{6}LiT, ^{7}LiH, ^{7}LiD, ^{7}LiT) have been investigated because of the availability of these materials in addition to the simplicity of the LiH structure, which resembles that of NaCl. The lithium hydride isotopes are viewed as the promising potential candidates for nuclear and high-density energy materials with application in many fields, such as nuclear power engineering, fuel hydrogen storage, and high- temperature superconductors (Zhang *et al.,* 2010). LiH is the lightest hydride, with 12.5% hydrogen content and 0.1 MPa equilibrium hydrogen pressure at 910°C. The Li^+ and H^- ions take on the closed-shell electronic configuration of the He atom. Consequently, the H ion may be considered as the

first ion in the halogen series, and LiH may be treated as one of the alkali halides.

Crystalline LiH has the sodium chloride structure; hence, there are two ions with four electrons contained in the primitive unit cell. The ambient phase has a cubic structure, which is much compressible and densely packed (Cazorla and Boronat, 2005). In addition, LiH is a strong reducing agent; it has a high hydrogen content, high melting point, low dissociation pressure due to its highly ionic nature that forms strong bonds with hydrogen, low density and it is a target for producing tritium (Dinh *et al.,* 2001). The simplified electronic structure of LiH has led to much theoretical interest in LiH.

LiH has a high affinity for moisture hence; it is highly reactive with water, which can cause difficulties in handling and use. This is because the reaction of LiH with water generates hydrogen gas and heat, the effects of which may be undesirable and pose compatibility or safety issues under certain circumstances.

Hydrolysis of LiH is exothermic and releases 90.7 kJ/mol of hydride (Yu and Lam, 1988). The chemical equation for this reaction is:

$$LiH_{(s)} + H_2O_{(l)} \longrightarrow LiOH_{(aq)} + H_{2(g)}. \tag{2.1}$$

Even in absence of a H_2O source, hydrogen generation from within the $LiH/Li_2O/LiOH$ structure has been reported (Dinh *et al.,* 2003). Table 2.1 shows the gravimetric hydrogen content of lithium hydride compared with a variety of actively researched hydrides. Certain borohydrides have higher weight densities, but many, such as sodium borohydride ($NaBH_4$) require complex catalysts, which are prone to degradation (Xia and Chan, 2005). Beryllium borohydride has very high hydrogen content but is too reactive and toxic to be considered (Soloveichik, 2007).

Table 2.1: Various hydrides and their gravimetric hydrogen content (Oxtoby *et al.*, 2007).

Hydride	**Gravimetric Hydrogen(percentage)**
NaH	4.1
CaH_2	4.7
$NaAlH_4$	7.4
$NaBH_4$	10.6
$LiBH_4$	18.4
LiH	12.5
$Be(BH_2)_4$	20.8

CHAPTER THREE

THEORY

3.1 Introduction

In this study, bulk, electronic, structural and thermodynamic properties of magnesium and lithium in both elemental and hydride forms have been systematically investigated and reported via the *ab-initio* pseudopotential total energy method.

The Latin term *ab-initio* means from the beginning and relies on basic and established laws of nature without additional assumptions or special models. Quantum mechanics is a set of principles that predicts how the particles behave, given the elementary properties such as the rest masses and charges. It is the most successful and powerful theory ever created. In the heart of this monumental scientific achievement lays the Schrödinger equation. In principle, by solving the Schrödinger equation one can access all the properties of a material of any size. However, the problem becomes practically unsolvable as the number of interacting particles increases, which is the case for most real-life situations.

The most appealing characteristic of *ab-initio* methods is that no experimental data are required in order to perform a calculation. The density-functional theory (DFT) technique enables computations on an accurate basis, and can be combined with molecular dynamics to solve problems within dynamical and thermodynamic phenomena at metal surfaces, such as premelting and blocked melting, atomic diffusion, and catalytic reactions (Jones and Gunnarsson, 1989).

3.2 Computational Theory

3.2.1 The Schrödinger Equation

In the year 1926, Erwin Schrödinger formulated a fundamental equation to describe the quantum aspects of matter. The many body form of the time independent Schrödinger equation consisting of M nuclei and N electrons is written as (Cuevas

and Scheer, 2010):

$$\hat{H}\psi_i(r_1, r_{2,...,}r_N, R_1, R_{2,...,}R_M) = E_i\psi_i(r_1, r_{2,...,}r_N, R_1, R_{2,...,}R_M), \tag{3.1}$$

where, $\hat{H}$ denotes the Hamiltonian, and ψ_i the wave function in terms of all the electronic (r) and nuclear coordinates (R).

In principle, the above equation is applicable to any physical system regardless of size (that is, from atoms to a whole crystal). In practice, however, a complete analytical solution is almost impossible for most real life systems, since the number of variables to deal with is determined by the 3(M + N) degrees of freedom. For example, if a methane molecule (chemical formula: CH_4) is considered, then there are in total 5 atomic nuclei and 10 electrons. The time independent Schrödinger equation, for a single methane molecule consequently becomes a partial differential eigenvalue problem in 45 variables. Although the exact solution of the Schrödinger equation is unsolvable for almost every real system, sensible approximations are used to make the most use of it (Cuevas and Scheer, 2010).

3.2.2 The Born-Oppenheimer Approximation

The Born-Oppenheimer approximation (Mayer, 2003) lightens the calculation of the energy and the wave function of moderate size physical systems by making use of the significant mass differences between the nuclei and the electrons. Considering the same example of a methane molecule mentioned in the previous section, it is seen that the mass of the nucleus is 2,800 times that of all the electrons surrounding it. It is therefore possible to decouple the motion of relatively slow moving nuclei and that of the fast moving electrons. In other words, the wave function of the system can be divided into electronic and nuclear components (Mayer, 2003):

$$\psi(r, R) = \psi_{electronic}(r, R) \times \psi_{nuclear}(R). \tag{3.2}$$

In the first step of the Born-Oppenheimer Approximation the nuclei are assumed

to have fixed positions, and the electronic Schrödinger Equation, which depends only on the electronic coordinates, is solved. For instance, the electronic wave function of the methane molecule depends on 30 electronic coordinates. It is assumed that for fixed nuclear positions the electrons are in their ground state. Consequently, the calculated electronic energies are functions of nuclear positions. In the second step of the Born-Oppenheimer approximation, these electronic functions serve to calculate a potential for the nuclear component of the Schrödinger equation. In the case of the methane example, it needs to deal with only 15 variables. To sum up, the nuclei move on the potential energy surface of the electronic ground state, and the electrons follow the nuclear motion adiabatically.

3.2.3 Density Functional Theory (DFT)

The problem is simplified by breaking down the Schrödinger equation into electronic and nuclear components, by the Born-Oppenheimer approximation. However, the electronic problem is still too complicated to be solved exactly due to the interactions between the electrons. Instead of using the 3N-dimensional Schrödinger equation for the many electron wave function, $\psi_i(r_1, r_{2...}r_N)$, Density Functional Theory (DFT) reduces the problem into a series of coupled one-body problems. This is accomplished by using the electronic density distribution, $n(r)$, and a universal functional of the density $E_{xc}[n(r)]$ (Engel and Dreizler, 2011).

3.2.3.1 Hohenberg-Kohn Theorem

P. Hohenberg and W. Kohn (Ayers *et al.,* 2006) proved that the construction of the total energy of a physical system could be expressed in terms of the electronic density. The ideas are related to earlier propositions of Thomas and Fermi in 1927, where atoms were modelled as systems with a positive potential (the nucleus) located in a uniform electron gas. The Hohenberg-Kohn theorem consists of two main parts:

Theorem 1 *In a system of N interacting particles under the influence of an external potential $V_{ext}(r)$, the ground state electron density, $n(r)$, uniquely determines*

the potential, $V_{ext}(r)$.

Since $n(r)$ determines $V_{ext}(r)$, then the full ground state Hamiltonian is known. Consequently, $n(r)$ completely determines all the properties of a physical system, such as the eigen functions, $\psi_i(r_1, r_{2,\ldots}, r_N)$ and the eigen values, E_i. In other words, the first theorem states that the energy is a unique function of the electron density:

$$E[n(r)] = F[n(r)] + \int V_{ext}(r)n(r)d^3r. \tag{3.3}$$

where, $E[n(r)]$ is a universal functional of the density, $F[n(r)]$ is a functional of density, V_{ext} is the external potential

Theorem 2 *There exists a function* $F[n(r)]$ *for the ground state energy, for any given* $V_{ext}(r)$. *The global minimum of this function defines the exact ground state energy of the physical system, and the density that minimizes the total energy is the exact ground state density,* $n_0(r)$.

Essentially, the second theorem states that the ground state electron density, $n_0(r)$, minimizes the universal functional, F, such that the electronic energy reaches its minimum value of $E[n_0(r)]$, that is,

$$E[n_0(r)] = F[n_0(r)] + \int V_{ext}(r)n_0(r)d^3r. \tag{3.4}$$

It should be noted that $F[n(r)]$ depends purely on the electron density. It does not depend on the external potential, $V_{ext}(r)$. The above two theorems together form the basis of DFT (Ayers *et al.,* 2006).

3.2.3.2 Kohn-Sham Equations

(Kohn and Sham, 1965) developed a set of differential equations in order to find the ground state density, $n_0(r)$. They started with the decomposition of the density functional given in (eq. 3.3) into three parts:

$$E[n(r)] = T_0[n(r)] + E_H[n(r)] + E_{xc}[n(r)] + \int V_{ext}(r)n(r)d^3r, \tag{3.5}$$

where $T_0[n(r)]$, $E_H[n(r)]$ and $E_{xc}[n(r)]$ define the kinetic energy, Hartree energy as a consequence of electron-electron repulsions, and exchange and correlation energies, respectively. The main idea behind the Kohn and Sham equations is to replace the kinetic energy of interacting electrons with that of an equivalent non-interacting system, and define E_{xc} such that the non-interacting system has the same ground state density as the interacting system. Within this assumption the electron density is given by the single particle wave functions, $\psi_{i,s,}$ where s labels the spin state,

$$n(r) = \sum_{s=1}^{2}\sum_{i=1}^{N} |\psi_{i,s}(r)|^2. \tag{3.6}$$

and accordingly the kinetic energy is described as,

$$T_0[n(r)] = \sum_{s=1}^{2}\sum_{i=1}^{N} \left\langle \psi_{i,s}(r)| - \frac{\nabla^2}{2}|\psi_{i,s}(r) \right\rangle. \tag{3.7}$$

where i is the initial number of electrons and N is the term for the number of electrons. Minimizing the total energy with respect to the single particle wave functions, under the constraint that this forms an orthonormal set, leads to the Kohn-Sham equations:

$$\left[-\frac{\hbar}{2m}\nabla^2 + V_{eff}(r)\right]\psi_{i,s}(r) = \epsilon_{i,s}\psi_{i,s}(r). \tag{3.8}$$

The problem of interacting particles is reduced to an equivalent problem of non-interacting particles. The effective potential used in the above (eq. 3.8) has the form:

$$V_{eff}(r) = e^2 \int \frac{n(r)}{|r - r'|}d^3r + \frac{\delta E_{ex}[n]}{\delta n(r)} + V_{ext}(r). \tag{3.9}$$

where $r - r^{'}$ is the distance between the two electrons. The above Kohn-Sham equations are just mathematical representations used to reduce the complexity of

the problem (Scheiner *et al.,* 1998). They need to be solved using a self-consistent procedure. Although the exact E_{xc} functional is not known, approximate functionals have been constructed that are universal in the sense that they do not depend on the materials investigated. Without the use of special basis sets and algorithms, the computational costs of solving the Kohn-Sham equations scale as N^3, where N represents the total number of Kohn-Sham orbitals.

3.2.4 Exchange and Correlation Functionals

The Kohn-Sham approach allows the calculation of the kinetic energy term in (eq. 3.5). The only undetermined component of the equation is the exchange-correlation energy functional, $E_{xc} = E_x + E_c$ (Koch and Holthausen, 2001). The exact form of this functional is not known and an approximate description is used instead. Efforts have focused on generating new exchange-correlation functionals to improve the accuracy of DFT. Computational results obtained with different functionals are directly compared to experiments so as to decide which functionals are to be used in a particular study. The details of the functionals used in this study are given in section 3.2.4.1.

3.2.4.1 Local Density Approximation (LDA)

In the local density approximation (LDA), general inhomogeneous electronic system is considered as locally homogeneous. For a spin-unpolarized system, local density approximation for the exchange-correlation energy is written as (Thijssen, 2007):

$$\mathbf{E}_{xc}^{LDA} = \int n(r)\epsilon_{xc}\left[n(r)\right] d^3r, \tag{3.10}$$

where n, and $\epsilon_{xc}[(n(r)]$ define the electron density and exchange-correlation energy per electron, respectively. Similarly, the exchange-correlation potential is written as:

$$V_{xc}(r) = \frac{\delta E_{xc}[n(r)]}{\delta n(r)} = \epsilon_{xc}[n(r)] + n(r)\frac{d\epsilon_{xc}[n(r)]}{dn(r)}. \tag{3.11}$$

LDA calculations usually describe the chemical trends correctly and are therefore quite useful in certain applications. The geometrical properties such as the cell parameters, bond lengths, and bond angles are also within a few percentages for systems involving covalent, ionic or metallic bonds. On the other hand, the binding energies are mostly overestimated. In LDA, the exchange correlation energy due to inhomogeneities in the electron density is ignored (Thijssen, 2007). Consequently, LDA has some limitations for very inhomogeneous systems, with the finite systems being the most obvious ones.

3.2.4.2 Generalized Gradient Approximation (GGA)

Generalized Gradient Approximation (GGA) uses the gradient of the charge density as a correction for deviations from the non-uniform charge density (Thijssen, 2007). The functional can be defined as a generalized form of (eq. 3.10) such that,

$$E_{xc}^{GGA} = \int n(r)_{xc}[n(r)]F_{xc}[n(r), \nabla n(r)]d^3r. \tag{3.12}$$

The term F_{xc} is dimensionless and numerous forms of it exist in literature. The most widely used forms were proposed by Perdew and Wang (PW91) (Perdew *et al.,* 1992) and Perdew, Burke, and Ernzerhof (PBE) (Perdew *et al.,* 1998). The calculations in this study make use of the Perdew and Zunger exchange correlational functional. Compared to LDA, GGA improves the binding energies, especially when there is chemical bonding between the atoms. Similar to LDA, screening of the exchange hole is not fully taken into account in GGA.

3.2.5 Pseudopotentials

Properties of physical systems are determined by their valence electrons rather than their core electrons. In an effort to simplify the computational cost of calculations, the ionic cores can be treated as frozen in their atomic configurations. The pseudopotential (also called effective potential) approach utilizes this idea by replacing

the core electrons and the strong ionic potential with a weaker pseudopotential that acts on a set of pseudo wave functions. Although the general ideas behind the pseudopotential approach are similar, there are several procedures to construct pseudopotentials, such as norm-conserving (Troullier and Martins, 1991) and ultra-soft (Laasonen *et al.,* 1993). In this study pseudopotentials will be used to represent the core and valence electrons (Kittel, 2005; Moyses *et al.,* 2005).

3.2.6 Bloch's Theorem

Felix Bloch, in the year 1928, developed a theorem that enabled the consideration of only the electrons within the unit cell to solve the Schrödinger equation (Kittel, 2005). The theorem states that the wave function of an electron within a perfectly periodic potential can be written as,

$$\psi_{nk}(r) = \mu_{nk}(r)e^{ik.r,}. \tag{3.13}$$

where k is the wave vector analogous to that of the wave vector in the theory of free electrons, r is a position vector, and $\mu_{nk}(r)$ is a periodic function that satisfies the boundary condition, $\mu_{nk}(r) = u_{nk}(r + R)$. The corresponding energy eigenvalue is,

$$\epsilon_n(k) = \epsilon_n(k + K), \tag{3.14}$$

where K is a reciprocal lattice vector. $\epsilon_n(k)$ is a continuous function, and since the energies associated with the index, n, vary with wave vector, k, this is known as an energy band. All distinct values of $\epsilon_n(k)$ are represented by k values within the first Brillouin zone of the reciprocal lattice.

3.2.6.1 Brillouin Zone Sampling

Bloch's theorem reduces the problem of calculating an infinite number of electronic wave functions to a finite number of wave functions for an infinite number of k-points (Kittel, 2005). In practice, one does not need an infinite number of k-points

since the electronic wave functions will be almost identical for k-points that are very close to each other. Therefore, a single k-point will be sufficient to represent the wave functions over a particular segment of k-space. In general, structures with high symmetry can be sampled with a reduced k-point set, since it is sufficient to consider the k-points only within the irreducible part of the Brillouin zone. Metallic systems require dense sets of k-points for a more accurate determination of the Fermi level. There exist several methods to generate suitable k-point sets and corresponding weights such as the uniform set of k-points (Monkhorst and Pack, 1976). Using k-point sets generated by such methods, an approximation of the electronic potential and total energy can be possible at a reduced computational cost.

3.2.6.2 Plane Wave Basis

In practice, the number of plane-waves used in a calculation is determined by (Thijssen, 2007):

$$\psi_k^n(r) = \frac{\sqrt{E_{cutoff} 2m_e}}{\hbar}, \tag{3.15}$$

where $\psi_k^n(r)$ is the plane wave, E_{cutoff} is the kinetic cut off energy. It is the only parameter that controls the accuracy of the plane wave basis set. Plane wave basis sets are mathematically simple, cover all the space equally without being biased to any particular region, and span the Hilbert space completely. In this sense, they are superior to local basis sets, especially when the initial form of the wave functions is unknown. The main disadvantage of a plane wave basis set compared to a local basis set is their computational cost which is abit high.

3.2.7 Thermodynamics

Thermodynamics is defined as a branch of science that deals with conversion of energy into work and heat and its relation to macroscopic variables such as temperature, volume and pressure. To address the thermodynamics of chemical processes, such as chemical reactions, one can make use of the mathematical methods of Josiah

Willard Gibbs (Klein, 1990). The Gibbs free energy of a system is defined as:

$$\triangle G = \triangle H - T\triangle S, \tag{3.16}$$

where H is the enthalpy, S is the entropy, and T is the absolute temperature. The change in the free energy of the system that occurs during a reaction measures the balance between the enthalpy and the entropy. Under constant temperature and pressure, if the change in the Gibbs energy from state A to state B is negative, then state B is said to be more thermodynamically stable than state A. At $T = 0$ K, the change in Gibbs energy equals the change in enthalpy, that is, $\Delta G = \Delta H$. The change in enthalpy is defined as the change in the internal energy of the system, ΔU, plus the work that the system has done on its surroundings, $P\Delta V$. Moreover the change in pressure and volume for reactions involving solids is negligible, mostly it is sufficient to focus upon the change in energy, ΔU, where U corresponds to the ground state energy of a system as calculated by DFT.

Phonon dispersions are used to determine the thermodynamic properties. The phonon dispersions are determined within the density functional framework and are used to calculate the free energy of the two metal hydrides within the quasiharmonic approximation (QHA) at each temperature T. The free energy at finite temperature has greater contributions from lattice vibrations (Maradudin *et al.,* 1971). In this approximation, the Helmholtz free energy $F(V,T)$ is given by:

$$F(V,T) = F_{static}(V) + F_{phon}(V,T), \tag{3.17}$$

where $F_{static}(V)$ is the energy of the static lattice at a given volume V and $F_{phon}(V,T)$ is the phonon free energy. F_{phon} can be expressed in terms of phonon density of states (DOS) as:

$$F_{phon}(V,T) = \sum_{qj} \frac{1}{2} h\omega_{qj}(V) + \kappa_B T \sum_{qj} ln \left[1 - exp\left(\frac{-h\omega_{qj}(V)}{\kappa_B T}\right)\right] \tag{3.18}$$

where $\omega_{qj}(V)$ is the frequency of the j^{th} phonon band at the point q in the Brillouin-zone. From $F(V,T)$ all thermodynamical behaviour can be deduced. The quasiharmonic approximation is known to work well for temperatures lower than the melting point of the system under investigation. The free energies are also used to calculate various thermodynamical properties within QHA. These include internal energy E, entropy S and the specific heat capacity at constant pressure C_P.

3.2.7.1 Zero-Point Energy Contribution (ZPE)

The lowest possible energy that a quantum mechanical physical system may have is called the zero-point energy (ZPE) (Einstein and Hopf, 1910). It arises as a result of nuclear motions. In molecular systems, both the vibrational and the rotational motions contribute to the ZPE. In solids, only the vibrational motions contribute. Within the harmonic oscillator approximation, the contribution of vibrational energies to the total energy term is calculated using the following equation (Einstein and Hopf, 1910):

$$E^{vib} = \int \left\{ \frac{\hbar}{2} + \hbar\omega n(\omega) \right\} g(\omega) d\omega, \tag{3.19}$$

where $(g)\omega$ is the phonon density of states, and $(n)\omega = \left[e^{\frac{\hbar\omega}{k_B T}} - 1 \right]^{-1}$ is the Bose-Einstein occupation number. At zero Kelvin, the ZPE contribution to the total energy is given by the first term of eq. 3.19 alone, whereas the second term represents the finite temperature contributions. Vibrational contributions to the entropy term can also be calculated when finite temperature results are demanded. The numerical calculation of ZPE can be accomplished using a dynamical matrix which is constructed via small displacements of atoms from their equilibrium positions and then finding differences of the accumulated forces (Einstein and Hopf, 1910). Each atom inside the cell is symmetrically displaced in its three degrees of freedom, by dr = $\pm$0.01 Å. To account for the spatial range of the dynamical matrix, the calculations require large super cells. ZPE contributions to the calculated total energies are considerable for light elements such as hydrogen. For heavy elements, the

phonon frequencies are low and accordingly the ZPEs are negligible.

CHAPTER FOUR

COMPUTATIONAL METHODOLOGY

4.1 Introduction

In this study, bulk, electronic and thermodynamic properties of MgH_2 and LiH have been studied via *ab-initio* pseudopotential plane wave method within the density functional theory (DFT). The Perdew and Zunger functional form of the local density approximation (LDA) was chosen for the electron exchange and correlation within DFT. All calculations in this study were based on density functional theory (Kohn and Sham, 1965) as implemented in the Quantum ESPRESSO (Q.E) computer code (Giannozzi *et al.,* 2009) which is a multi-purpose, multi-platform software for *ab-initio* calculations of periodic and disordered condensed matter systems within a plane wave basis set. Quantum ESPRESSO stands for Quantum-opEn-Source Package for Research in Electronic structure, Simulation and Optimization. QE uses plane wave basis sets for the expansion of the electronic wave function, a pseudopotential description of the electron-ion interaction and density functional theory (DFT) for description of electron-electron interactions.

Electron-ion potential was described by means of ultrasoft pseudopotentials (USPP) (Vanderbilt, 1990). USPP are transferable and smooth, ensuring rapid convergence in the calculated total energy of the system and by extension achieves rapid convergence of the system properties with respect to an increase in the plane wave basis set. The PZ form of the LDA was used to treat the exchange and correlation energies in electronic structure calculations. In plane wave self-consistent field (pwscf) and relaxation calculations, geometry optimizations were performed using the Broyden-Fletcher-Goldfarb-Shanno (BFGS) algorithm, an algorithm in-built in the Q.E code.

4.2 k-point Sampling

First-principles total energy calculations require integrals of wave functions and/or eigenvalues over the Brillouin zone. Electronic states are only allowed at a set of k-points determined by the boundary conditions that apply to the bulk solid. The density of allowed k-points is proportional to the volume of the solid. An infinite number of k-points accounts for the infinite number of electrons in the solid, and only a finite number of electronic states are occupied at each k-point. The Bloch theorem changes the problem of calculating an infinite number of electronic wave functions to one of calculating a finite number of electronic wave functions at an infinite number of k-points (Kittel, 2005).

The occupied states at each k-point contribute to the electronic potential in the bulk solid so that, in principle, an infinite number of calculations are needed to compute this potential. However, the electronic wave functions at k-points that are very close together will be almost identical as mentioned before, hence, it is possible to represent the electronic wave functions over a region of k-space by the wave functions at a single k-point. In this case the electronic states at only a finite number of k-points are required to calculate the electronic potential and hence determine the total energy of the solid.

Methods have been devised for obtaining very accurate approximations to the electronic potential and the contribution to the total energy from a filled electronic band, by calculating the electronic states at special sets of k-points in the Brillouin zone according to (Chadi and Cohen, 1973; Joannopoulos and Cohen, 1973; Monkhorst and Pack, 1976; Evarestov and Smirnov, 1983).

In this study, special k-points were generated manually and optimized for all calculations to ensure their accuracy in this study. Some k-points were generated automatically using the Monkhorst-Pack scheme (Monkhorst and Pack, 1976) which ensures that the irreducible part of the Brillouin zone (IBZ) is integrated over a set (mesh) of uniformly spaced k-points.

4.3 Modelled and Relaxed Mg, MgH_2 and LiH

Bulk properties of MgH_2 have been studied to understand its most basic properties. This was in line with the intention to study the bonding and hybridization in the compounds as well as other properties of interest.

Bulk magnesium has the hexagonal close packed structure, which is specified by a lattice parameter (a) and the ratio $\frac{c}{a}$ of the vertical axis to one of the horizontal axis. MgH_2 has a TiO_2-rutile tetragonal symmetry (P42/mnm, group No. 136) structure with experimental lattice parameters being $a = b = 4.501$ Å and $c = 3.010$ Å (Noritake *et al.,* 2003). From basics of energetics, every system tries to be in a state of minimum energy (ground state), which is obtained by minimizing equation 3.9 to self-consistency with respect to a set of orbitals ψ_i, and to an accuracy ranging from 10^{-6} to 10^{-8} Ry depending on the system under investigation.

In addition, structural relaxation was done to determine the local minimum of $\upsilon(r_i)$ as a function of position r_i. Minimization of the energy of a system with respect to both k-points and plane wave energy cut off was performed to compare the stability of different structures. Bulk properties were calculated after optimizing k-points and the cut off energy. The total energy of free atoms, in this case H and Mg was calculated by placing a single atom at the origin (0 , 0 , 0) a_0 in a large cubic box of sides 15 Bohr, then allowed to relax. This large size of the box ensured that they were approximated as if they were completely free. 15 Bohr was chosen after several calculations were done by varying the size of the cubic box from 10 Bohr, 15 Bohr, 20 Bohr, 25 Bohr to 30 Bohr. Of all the calculations, the box of size 15 Bohr emerged as the best suited for the kind of calculation.

4.4 Minimization of the Kohn-Sham Energy Functional

For any calculation, electronic states that minimize the Kohn-Sham energy functional must be found. According to Payne *et al.,* (1992), there is an infinite number of K-S Hamiltonians, each of which has different sets of eigenstates. One of these

sets of eigenstates, the set generated by the self-consistent K-S Hamiltonian, minimizes the K-S energy functional. The K-S energy functional therefore has a single well-defined energy minimum (Blaha *et al.,* 2010). The iteration process within Quantum Espresso code used in this study ensured that the calculated minimum energy was always compared to the Harris Foulkes energy for the different systems, so as to establish how accurate the system had converged. Energy minimization was done using the conjugate gradient method while diagonalization was done using the Davidson diagonalization with overlap (Payne *et al.,* 1992).

4.5 Solving the Self Consistent (SCF) Kohn-Sham Equation

In (eq. 3.9) the effective potential depends on the electron density $n(r)$, which in turn depends on the Kohn-Sham orbitals $\psi_i(r)$, which are being searched. It then means that the Kohn-Sham equation has to be solved iteratively until a self-consistent solution is reached. The schematic diagram of the procedure is shown in Figure 4.1.

4.6 Structural Optimization

The choice of pseudo potential cut off energy for the plane wave basis and k-points for the Brillouin zone (BZ) are the three most important factors that determine the quality of the numerical calculations. Reliable results can only be obtained if accurate cut-offs and dense k-points are used. E_{cut} purely depends on the chemical elements used in the calculations. Structural optimization was done using convergence tests for k-point mesh and the total energy cut off. The optimized values for the k-point mesh and the total energy cut off were then used to obtain the optimized lattice parameters.

Structural parameters for both Mg and MgH_2 were optimized. Here, the atoms were allowed to relax in either x, y and z directions until the systems achieved the minimum energy positions. The relaxed atomic positions were then used to optimize both the plane wave energy cut off and the k-point grid. Optimal values of the plane

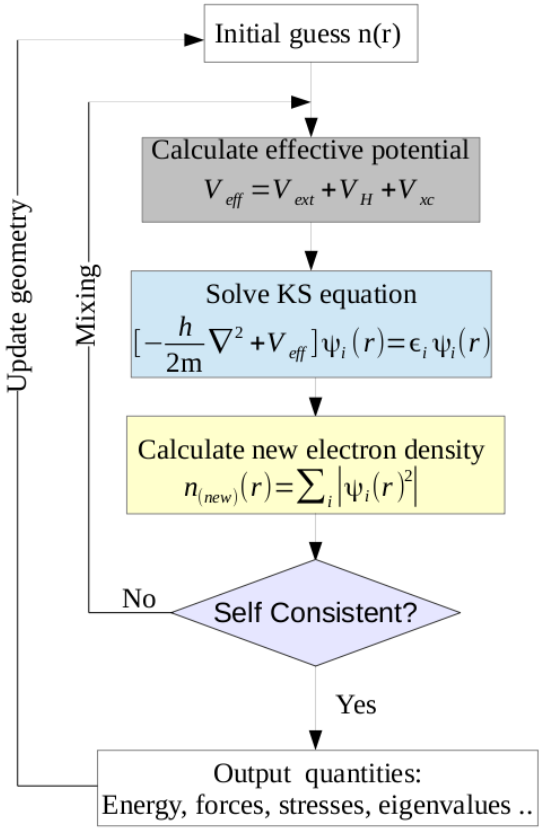

Figure 4.1: Schematic representation of the self-consistent loop for the solution of Kohn Sham equation (Kresse and Furthmuller, 1996).

wave cut off energy and the k-points were used to minimize the total energy as a function of the cell volume. This was done by varying the cell volume by ±15, ±13, ±10, ±7 and ± 5 % of the experimental volume V_0.

The structural properties such as lattice equilibrium constant (equilibrium volume V_0), bulk modulus and ground state energy E_0 were obtained from the total energy and fitted to the Murnaghan equation of state (Tyuterev and Vast, 2006). The converged k-point mesh was then used to calculate the total cut off energies (E_{cut}) and volumes (V).

Modelled bulk Li and LiH were used to optimize some of the parameters that were used for DFT calculations. Just like in the case of Mg and MgH_2, experimental parameters were used as the starting points to model both the Li and LiH structures. Modelled bulk LiH has a simple rock salt structure with face-centred cubic (FCC) structure belonging to the space group Fm-3m. The primitive cell consists of two

atoms, with the Li atom in the 2a (0, 0, 0) wyckoff position and H atom occupying the 2c ($\frac{1}{2}$, $\frac{1}{2}$, $\frac{1}{2}$) wyckoff site with an experimental lattice constant of $a = b = c =$ 4.083 Å (Kittel, 2005). The structural properties of LiH were calculated from the optimized structures. The equilibrium volume of ground-state was determined by calculating the total energy per primitive unit cell as a function of volume.

4.6.1 *k*-points and Plane Wave Energy Cut Off Optimization

Using the experimental lattice parameter of $a = 3.21$ Å and $c = 5.21$ Å for bulk Mg and $a = 4.501$ Å and $c = 3.01$ Å (Noritake *et al.,* 2003), the *k*-points were then optimized. The cut-off energy was fixed at 30 Ry to make the calculation less computationally expensive during the test runs. *k*-points were varied from a 2×2×2 grid to higher values 25×25×25. The values of minimum energies obtained with respect to the corresponding *k*-point grids were then plotted for both Mg and MgH_2. These values of *k*-points were then used in all subsequent calculations.

For LiH, Brillouin-zone integrations were performed on the Monkhorst–Pack *k*-point mesh (Monkhorst and Pack, 1976). The Monkhorst Pack scheme ensures that the irreducible part of the Brillouin Zone is integrated over a set (mesh) of uniformly spaced *k*-points. Using the experimental lattice parameter of $a = b = c = 4.083$ Å for bulk LiH, the *k*-points were then optimized. The cut off energy was fixed at 30 Ry to make the calculation less computationally expensive during the test runs. *k*-points were varied from a 2×2×2 grid to higher values. The values of minimum energies obtained with respect to the corresponding *k*-point grids were then plotted for LiH. This value of *k*-points was then used in all subsequent calculations.

The converged *k*-point mesh was then used to calculate the total cut off energies (E_{cut}). This procedure was carried out after optimizing the *k*-points.

4.7 Phonons and Thermodynamic Properties

Since DFT provides us with the total energy, as a function of the atomic positions, it can be used to calculate the vibrational spectra of a solid. By occupying the

obtained spectrum according to Bose-Einstein statistics, one can additionally obtain information on the thermodynamical properties of a material (Einstein and Hopf, 1910). In the direct method, the vibrational spectra are calculated by displacing the ions finite distances from their equilibrium positions. In principle, each atom has to be displaced in three linearly independent directions. Using the symmetry of the crystal, the number of displacements can usually be decreased significantly. The calculated forces caused by these displacements are then used to construct the force constant matrix. The force matrix is then used to calculate the thermodynamic properties such as the internal energy, entropy, heat capacity and vibrational energy (Einstein and Hopf, 1910).

CHAPTER FIVE

RESULTS AND DISCUSSION

5.1 Introduction

This chapter gives computational results of the most essential properties of the two metal hydrides considered in this study. The chapter also analyzes and discusses the results obtained and their comparison to experimental results and other theoretical calculations. As earlier mentioned, apart from LiH being a possible candidate for hydrogen storage, it is also studied because it is the simplest in terms of its low molecular weight, while MgH_2 is one of the most important compounds for the reversible storage of hydrogen because of its ability to store large amounts of hydrogen, its light weight as well as low cost compared with other potential sources of hydrogen.

5.2 Structural Optimization

5.2.1 Bulk Mg and MgH_2

Modelled bulk Mg and MgH_2 structures were used to optimize some of the important parameters that were used for the DFT calculations. The results obtained from the theoretical calculations were then compared with those from other works and experimental findings in order to give the work the authenticity it desired to eliminate any ambiguities. In modelling both the Mg and MgH_2 structures, experimental values were used to obtain the initial coordinates of the atoms. Figure 5.1 shows the optimized hexagonal close packed structure of bulk Mg, which was visualized using the XCrysDen programme (Kokalj, 2003). Figure 5.2 shows the optimized tetragonal crystal structure of MgH_2.

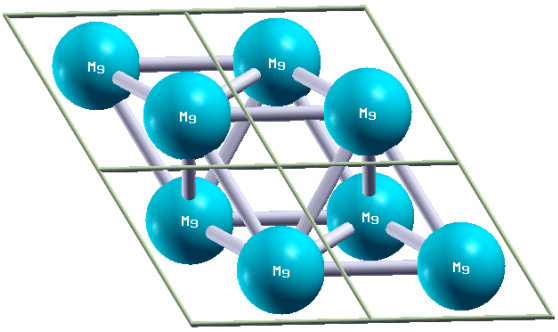

Figure 5.1: Optimized hexagonal structure of bulk Mg.

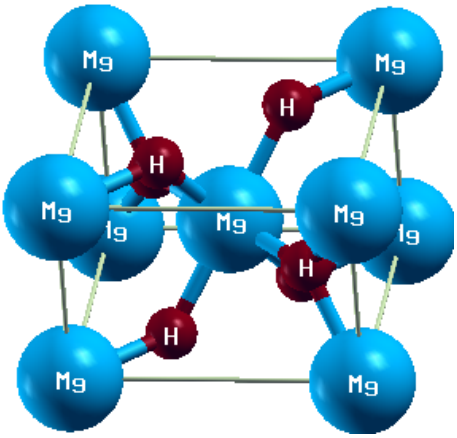

Figure 5.2: Optimized tetragonal crystal structure of MgH_2.

5.2.1.1 *k*-points Optimization

Brillouin-zone integrations were performed on the Monkhorst–Pack k-point mesh (Monkhorst and Pack, 1976). The Monkhorst Pack scheme ensures that the irreducible part of the Brillouin Zone is integrated over a set (mesh) of uniformly spaced k-points. Using the experimental lattice parameter of $a = b$ 3.21 Å and $c = 5.21$ Å for bulk Mg and $a = b$ 4.501 Å and $c = 3.01$ Å (Noritake *et al.,* 2003) for bulk MgH_2, the k-points were then optimized. The cut-off energy was fixed at 30 Ry to make the calculation less computationally expensive during the test runs. k-points were varied from a 2×2×2 grid to higher values of 25×25×25. The values of minimum energies obtained with respect to the corresponding k-point grids were then plotted for both Mg and MgH_2. The converged k-point meshes were found to be 10×10×10 for Mg and 4×4×6 for MgH_2, respectively. These values of k-points were then used

in all subsequent calculations. Figure A 1 in appendix A shows a k-point mesh plot against energy for Mg, while figure A 2 shows the plot of k-point mesh against energy plot for MgH_2. The converged k-point mesh was then used to calculate the total cut off energies (E_{cut}) and volumes (V).

5.2.1.2 Optimization of the Plane Wave Cut Off Energy

This step was done after optimizing the k-points. An optimum value of 80 Ry was chosen for MgH_2 and 30 Ry for Mg since the energies were well converged around this energy to an accuracy of 10^{-12} Ry. Figures A 3 and A 4 in appendix A show the plot for the computed total energies with different plane-wave cut-off energies for Mg and MgH_2, respectively.

5.2.2 Optimized Crystal Structure of LiH

Figure 5.3 shows the structure of LiH. It has a simple rock salt structure with face-centred cubic (FCC) structure belonging to the space group Fm-3m. The primitive cell consists of two atoms, with the Li atom in the 2a (0, 0, 0) wyckoff position and H atom occupying the 2c ($\frac{1}{2}$, $\frac{1}{2}$, $\frac{1}{2}$) wyckoff site.

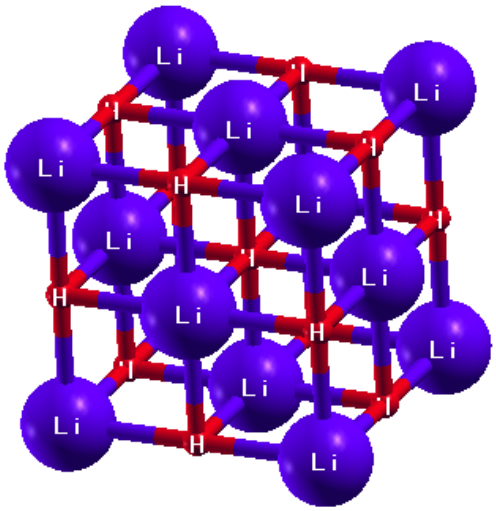

Figure 5.3: Modelled crystal structure of LiH showing the rock salt structure.

5.2.2.1 k-points Optimization

For LiH, Brillouin-zone integrations were performed on the Monkhorst–Pack k-point mesh (Monkhorst and Pack, 1976). The Monkhorst Pack scheme ensures that the irreducible part of the Brillouin Zone is integrated over a set (mesh) of uniformly spaced k-points. Using the experimental lattice parameter of $a = b = c = 4.083$ Å for bulk LiH, the k-points were then optimized. The cut off energy was fixed at 30 Ry to make the calculation less computationally expensive during optimization of the k-points. k-points were varied from a 2×2×2 grid to higher values of 12×12×12. The converged k-point mesh was found to be 4×4×4, which was kept fixed for all other subsequent calculations. Figure A 5 in appendix A shows a plot of the k-point mesh against energy for LiH.

5.2.2.2 Plane Wave Cut Off Energy Optimization for LiH

An optimum value of 30 Ry was chosen for LiH since the energies were well converged around this energy to an accuracy of 10^{-12} Ry. This value was fixed for all other subsequent calculations. Figure A 6 in appendix A shows a plot of the optimized total energy for LiH against the plane wave cut off energy.

5.3 Equilibrium Bulk Properties

Equilibrium bulk properties considered in this study include the equilibrium lattice constant (a_0), the bulk modulus (B_0), and the pressure derivative of the bulk modulus ($B_0^{'}$). The properties were obtained following a rigorous system relaxation of the electronic structures for the respective metal hydrides. The results were compared with other calculations for each metal hydride as well as experimental values where available. All the calculations reported in this study were carried out at ground-state ($T = 0$ K), while normally most experiments are done at elevated finite conditions of temperature and pressure.

5.3.1 Mechanical Properties of MgH_2

Table 5.1 shows the mechanical properties of MgH_2. These include the lattice constant, a_0 which corresponds to the size of a conventional unit cell length at equilibrium volume, V_0. It was obtained by minimizing the total energy as a function of the cell volume. The bulk modulus B_0 and its pressure derivative $B_0^{'}$ were obtained by fitting the energy-volume, $(E - V)$, data to the Murnaghan equation of state. The bond lengths were determined by viewing the relaxed structures using Xcrysden visualization programme.

Table 5.1: Optimized lattice parameters and bulk modulus(B_0) of Magnesium Hydride.

MAGNESIUM HYDRIDE				
	Calculated	**Experimental**	**Other theoretical works**	**% deviation from experimental**
a (Å)	4.540	$4.501^a, 4.500^b$	$4.515^d, 4.520^e$	+0.8665
c (Å)	3.019	$3.010^a, 3.010^b$	$3.019^d, 3.010^e$	+0.2990
B_0 (GPa)	56.85	NV	$55.50^f, 57.00^{b,g}$	NO
Mg-H (Å)	1.95	1.96^c	NO	−0.5102

NV-not available, NO-not obtained
[a] Noritake *et al.,* 2003, [b] Moyses *et al.,* 2005, [c] Sato *et al.,* 2006, [d] Novaković *et al.,* 2009, [e] Van Setten *et al.,* 2007, [f] Pozzo and Alfe, 2008 and [g] Kanagaprabha *et al.,* 2012.

From the study, lattice constants of $a = 4.540$ Å, $b = 4.540$ Å and $c = 3.019$ Å for magnesium hydride were obtained, which differed only by less than ±1% when compared to the experimental values of $a = 4.501$ Å and $c = 3.01$ Å (Noritake *et al.,* 2003). The calculated lattice constants a and b were slightly overestimated by + 0.8665% from the experimental lattice constant while that of c was overestimated by + 0.2990% indicating a general lengthening of both the lattice constants. The bond length Mg–H was found to be 1.95 Å, a value that was in close agreement with the experimental value of 1.96 Å (Sato *et al.,* 2006). The bond length Mg–H was underestimated by − 0.5102% from the experimental value. For the bulk modulus,

no experimental data has been reported for comparison to the best of my knowledge. The calculated bulk modulus compared quite well from other theoretical works, whereby values of 55.50 GPa (Pozzo and Alfe, 2008) were obtained for MgH_2 while the calculated value was 56.85 GPa. The calculated parameters in this work are in agreement with those of other works (Van Setten *et al.,* 2007; Noritake *et al.,* 2003; Kittel, 2005; Moyses *et al.,* 2005; Novaković *et al.,* 2009; Pozzo and Alfe, 2008; Kanagaprabha *et al.,* 2012) as seen in Table 5.1.

5.3.2 Mechanical Properties of LiH

Bulk LiH has a simple rock salt structure which is face-centred cubic (FCC) belonging to the space group Fm-3m. Its optimized bulk properties were obtained by minimizing the total energy as a function of the cell volume, followed by a fitting process of the energy-volume $(E - V)$ data to the Murnaghan equation of state. Results obtained from the calculations for bulk LiH in comparison to other works and experimental works are shown in Table 5.2. The calculated lattice parameters were $a = b = c = 3.93$ Å for lithium hydride.

Table 5.2: Optimized lattice parameters and bulk modulus (B_0) for Lithium Hydride.

LITHIUM HYDRIDE				
	Calculated	**Experimental**	**Other theoretical works**	**% deviation from experimental**
a (Å)	3.93	4.0830[a,b]	4.0130[e], 3.9976[c]	−3.7470
B_0 (GPa)	39.9000	32.2000[c], 34.2400[d]	36.0705[e]	+10.83, +17.40

[a] Kittel, 2005, [b] Herbst and Hector, 2005, [c] Loubeyre *et al.,* 1998, [d] Gerlich and Smith, 1974 and [e] Bouhadda *et al.,* 2007.

The results of this study show that while the lattice constants contracted, the bulk modulus varied by between + 10.8% and + 17.4% of the two reported experimental values, respectively. The reported experimental bulk moduli of LiH are 32.2

and 34.2 GPa, showing that the calculated bulk moduli of LiH is slightly overestimated due to the pseudopotentials used. On the other hand, it must be kept in mind that the calculated data are obtained under absolute zero temperature, and the experimental data are obtained mostly at room temperature which is easy to understand from the fact that increasing temperature leads to an increase in the equilibrium volume, and hence to a decrease in the bulk modulus (Wang, 2008).

The relatively close agreement of the equilibrium properties with the experimental values confirms the findings of this work and the fact that what has been modelled is indeed a true representation of what has been done experimentally. This gives us the confidence in achieving a higher level of accuracy in all the subsequent calculations. It reflects the reliability of the self-consistent calculations and the used pseudo potentials.

5.4 Electronic Properties

5.4.1 Band Structure (BS) and Density of States (DOS)

To analyze the electronic structure of both MgH_2 and LiH, the BS and DOS have been calculated. DOS is very useful in analyzing the relationship between the electronic structure and the bonding of hydrogen storage compounds. A zero DOS for an energy level means that no states can be occupied while a high DOS for an energy level represents that many states are available for occupation. DOS gives invaluable information about the bonding within solids and in classification of materials as metallic, semiconducting or insulating (Kittel, 2005). Metals have non-localized electrons and no electronic band gap (separation between valence and conduction band). Those materials with a large gap ≥ 4 eV are called insulators while systems with a smaller gap are categorized as semiconductors. In this study, DOS for hydrogen, lithium and magnesium atoms located within the bulk as well as for MgH_2 and LiH have been considered.

5.4.1.1 Band Structure (BS) and Density of States (DOS) for MgH_2

Figure 5.4 shows the high symmetry points and the path Γ-X-M-Γ-Z-R-A-Z in the primitive Brillouin zone that was used to plot the band structure for MgH_2 as generated using XCrysDen programme.

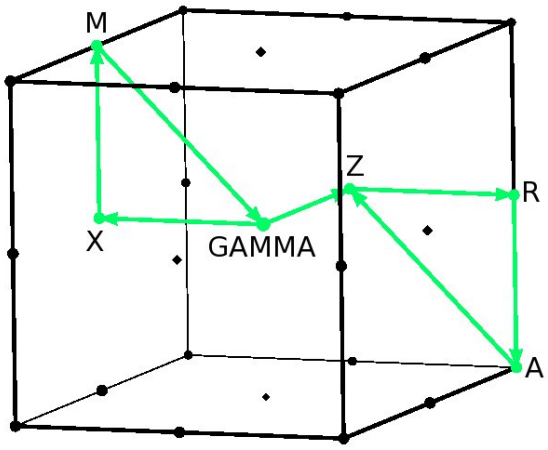

Figure 5.4: High symmetry path Γ-X-M-Γ-Z-R-A-Z in the primitive Brillouin zone for MgH_2.

Figure 5.5 shows the DOS and BS of bulk MgH_2, whereby the band structure was plotted along the high symmetry path Γ-X-M-Γ-Z-R-A-Z.

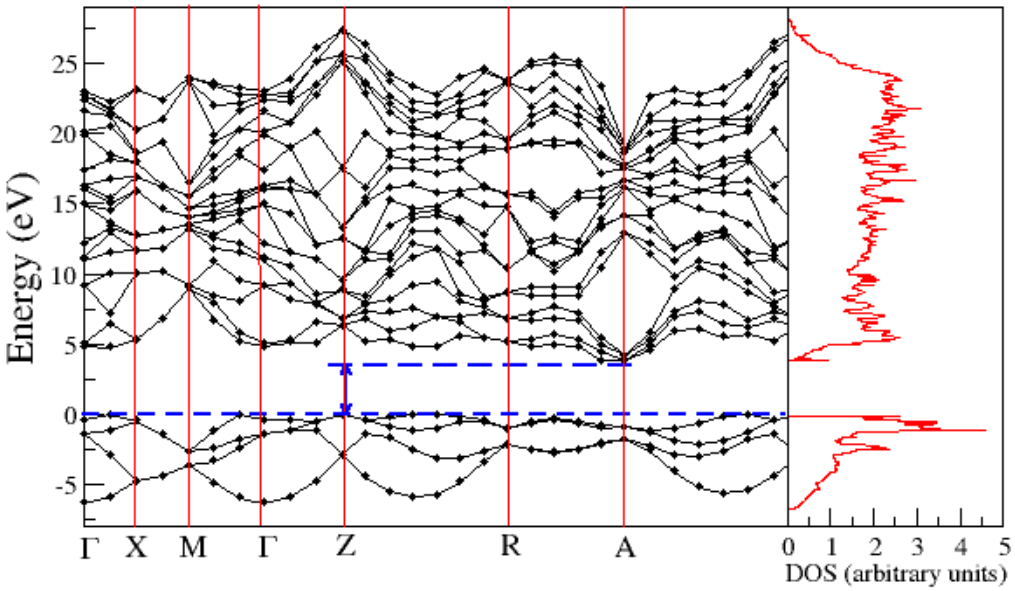

Figure 5.5: Calculated BS and DOS for Magnesium Hydride along the high symmetry path of Γ-X-M-Γ-Z-R-A-Z.

Both the DOS and BS, respectively, showed that the electronic states of magne-

sium hydride were constituted of narrow valence bands and broad conduction bands. They also correlate quite well in such a way that high DOS corresponds to more bands within the band structure while low values correspond to fewer energy states available for occupation. Rutile MgH_2 has a wide indirect band gap of 3.65 eV occuring from Z to A suggesting that the material is an insulator. This is much narrower than the experimental value which is 5.16 eV (Yu and Lam, 1988), although the value obtained in this study was in agreement with that of other theoretical studies by Bouhadda *et al.,* (2007) of 3.6 eV. This underestimation of the energy gap can be attributed to the well known property of DFT calculations which tends to underestimate the fundamental gap (Sholl and Steckel, 2011).

5.4.1.2 Band Structure and Density of States for LiH

Figure 5.6 shows the high symmetry points and path Γ–X–W–L-Γ–K-X in the primitive Brillouin zone that was used to plot the band structure for LiH as generated using Xcrysden programme.

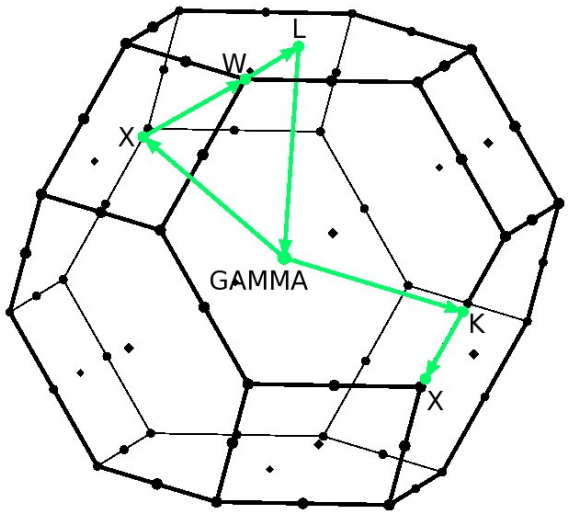

Figure 5.6: High symmetry path Γ–X–W–L-Γ–K-X in the primitive Brillouin zone for LiH.

Based on the computed equilibrium lattice parameter, the electronic energy band structure and density of states for LiH was also plotted as shown in Figure 5.7. The band structure for LiH was plotted along the high symmetry axes in the BZ in the energy region from − 9 to 25 eV, while the Fermi level (E_f) was set at zero

energy. The calculated energy band gap was found to be 3.0 eV which was in good agreement with another calculated value of 3.2 eV (Bouhadda *et al.,* 2007). This shows that LiH is an insulator with a wide direct band gap located at X. The experimental energy band gap is 4.99 eV for bulk LiH at $T = 4.2$ K indicating that the value obtained in this study is underestimated by 39.88%. Just like in the case of MgH_2 underestimation of the energy band gap is due to the well known limitations of DFT. This is due to the fact that DFT calculations greatly overemphasize the stabilization provided by delocalization, hence wavefunction stability, thereby leading to this underestimation. The broad band arises from the equivalence of the Li 2s and hydrogen 1s orbitals in energy and geometry, allowing for a significant hybridization (Smithson *et al.,* 2002). Figure 5.7 shows the electronic band structure along the Γ–X–W–L-Γ–K-X high symmetry path and total DOS for LiH.

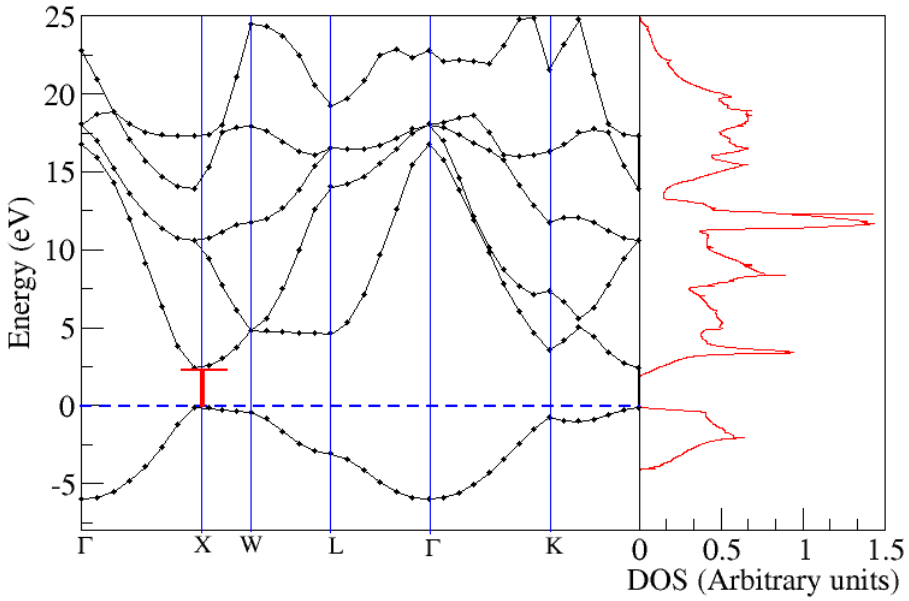

Figure 5.7: Electronic band structure along the Γ–X–W–L-Γ–K-X high symmetry path and total DOS for LiH.

5.4.2 Projected Density of States (PDOS)

Density of states are very useful for analyzing the relationship between the electronic structure and the bonding of different materials. In particular, projected density of states gives us more information on the contribution of each orbital, especially in

the case of the two metal hydrides.

5.4.2.1 Projected Density of States (PDOS) for MgH_2

Figure 5.8 shows the PDOS for Magnesium Hydride. The bonding in MgH_2 is dominantly ionic; occupied hydrogen orbitals give the main contribution to the valence states, whereas the conduction bands have a significant contribution from the Mg orbitals. This is shown by the fact that the valence band consists predominantly of H-1s and Mg-3p states, while Mg-3s electrons are almost completely transferred to surrounding H atoms with lower energies in the valence band. Features of valence band close to Fermi level are influenced also by a small amount of covalent H–H contribution. Stability of a compound is proportional to the number of states at the Fermi level from H-1s states, thus, in typical density of states, bonding and anti-bonding electronic states are separated by a region with a small number of states or even an energy gap. Stable compounds have Fermi level positioned in this region. Movement of the Fermi level towards higher energy means that significant number of anti-bonding states is incorporated in bonding, which leads to lowering of compound stability.

5.4.2.2 Projected Density of States (PDOS) for LiH

The projected density of states (PDOS) for LiH is plotted in Figure 5.9 whereby the energy region is considered from $-$ 6 to 26 eV. From Figure 5.9, the participation of Li cations to the conduction band is larger. As the conduction band moves towards the symmetry point X, it is lowered in energy because here the Li-2p states participate in a bonding combination with hydrogen states. The conduction band minimum at the L-point is raised in energy because the lithium states contribute to an anti-bonding combination with hydrogen states (Miwa *et al.,* 2004). The contribution of DOS around the Fermi energy comes from the 1s orbital of H as well as 1s and 2p orbitals of Li. The 1s states contribute to the valence band while 2p orbitals contribute to the conduction band. 1s and 2p orbitals are indicative of

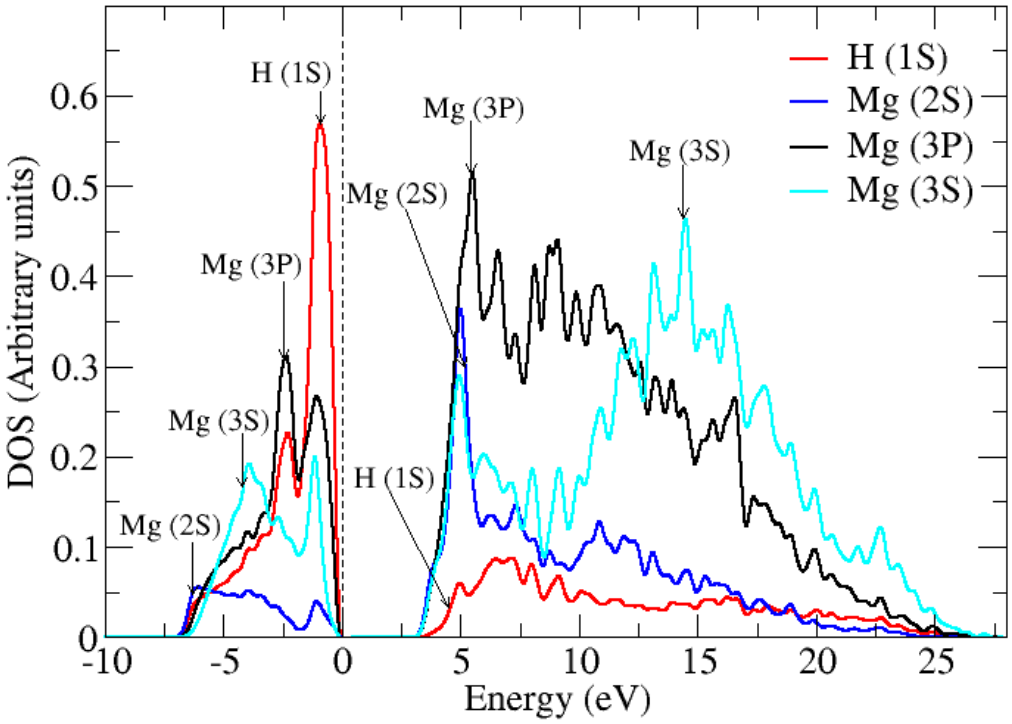

Figure 5.8: Projected density of states for bulk Magnesium Hydride.

hybridization during bonding of the crystal. LiH is not only an ionic crystal, but also has some covalent bonds.

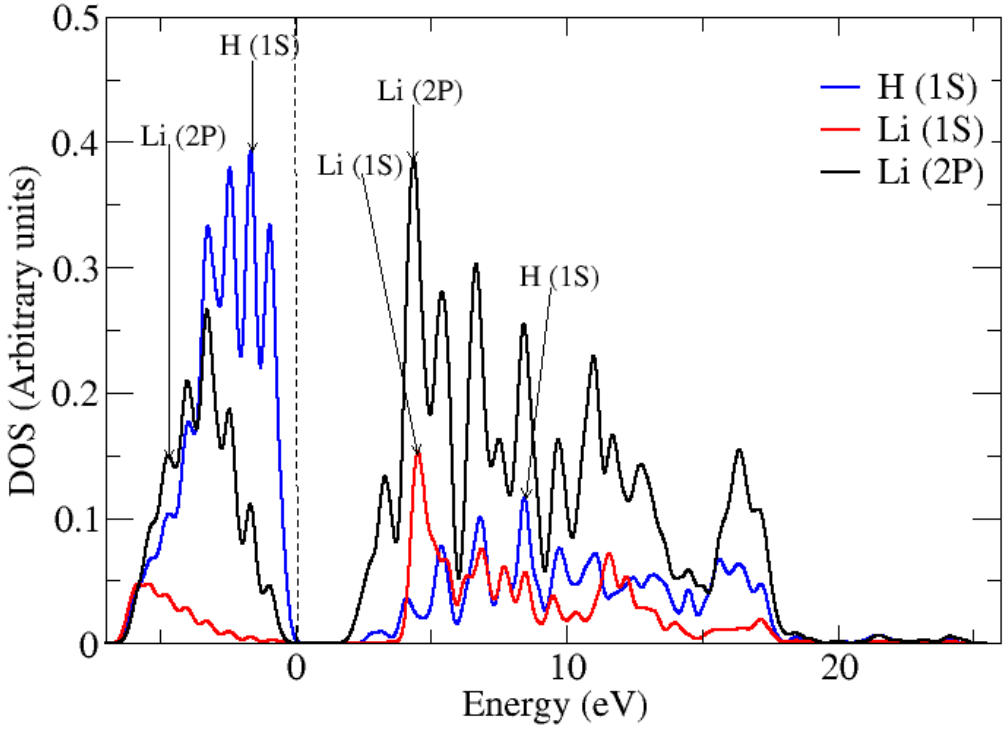

Figure 5.9: Projected density of states for Lithium Hydride.

5.5 Cohesive Energy

The cohesive energy (E_{coh}) of a crystal is defined as the energy that must be added to the crystal to separate its components into neutral free atoms at infinite separation, with the same electronic configuration at 0 K and 1 atmosphere (Kittel, 2005). It is taken to be the difference between the total energy of the crystal and those of the isolated atoms. In the bulk material, cohesive energy may be used as a pointer to the formation of the crystal, while in surface calculations, cohesive energy is the energy required to remove an adsorbed atom.

5.5.1 Cohesive Energy of MgH_2

For the binding energy of the MgH_2 crystal, a spin-polarized calculation for the H atom as parameterized by Perdew and Zunger (Ceperly and Alder, 1980; Perdew and Zunger, 1981) was performed. The calculated total energy of the H atom was found to be − 0.9522 Ry. Figure 5.10 illustrates a hydrogen atom placed in a large box of side 15 Bohr to make sure that the atom is completely free.

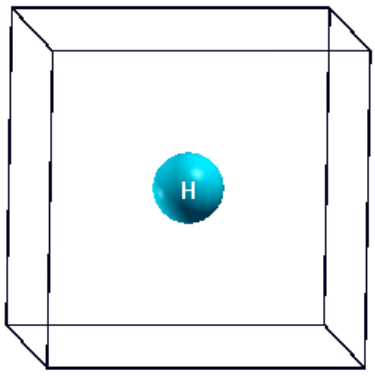

Figure 5.10: Hydrogen atom placed in a large box of side 15 Bohr to make sure that the atom is completely free.

The cohesive energy was calculated according to equation 5.1,

$$E_{coh} = -\frac{[E_{bulk} - N(E_{atom})]}{N} \times -13.6\ eV. \tag{5.1}$$

Where E_{bulk} is the total energy of the bulk matrix, E_{atom} is the energy of an isolated

free atom and N is the effective number of atoms in the unit cell which was used in optimizing bulk MgH_2. For the specific case of MgH_2, the equation can be represented as;

$$E_{coh} = -\frac{E_{MgH_2} - [E_{Mg} - E_H]}{6} \times -13.6\ eV. \tag{5.2}$$

Where E_{coh} is the cohesive energy of MgH_2, E_{MgH_2} is total energy of the bulk MgH_2, E_{Mg} is the energy of an isolated free Mg atom and E_H is the energy of a free hydrogen atom placed in a large cubic box. The effective number of atoms in the bulk unit cell is 6. The cohesive energy of MgH_2 therefore can be computed as,

$$E_{coh} = -\frac{8.968Ry - [-2.0154Ry - 0.9522Ry]}{6} \times -13.6\ eV = 13.6009\ eV/\text{unit cell}. \tag{5.3}$$

The cohesive energy of 13.6009 eV per unit cell of MgH_2 does not include the vibrational energy of the solid. The experimental cohesive energy is 13.4 eV per unit cell (Yamaguchi *et al.*,1994). The difference between the calculated theoretical value and the experimental value is +1.499% which indicates over binding and hence good agreement between theory and experiment. Cohesive energy is a very critical aspect in the hydrogen storage materials and in particular MgH_2. This is because hydrogen is stored in the bulk, and for it to be used for practical applications, it will need to be desorbed from the bulk to the surface. The binding/cohesive energy of 13.6 eV is very high and this means that a lot of energy will be needed to remove a hydrogen atom from the bulk of MgH_2. The high value of the binding energy gives an indication of how much energy needs to be added so as to reduce it and thus make it easier to remove a hydrogen atom or molecule from the bulk.

5.5.2 Cohesive Energy of LiH

The cohesive energy of LiH was calculated using the formula below:

$$E_{coh} = -\frac{E_{LiH} - [E_{Li} - E_H]}{2} \times -13.6eV. \tag{5.4}$$

Where E_{coh} is the cohesive energy of LiH, E_{LiH} is total energy of the bulk LiH, E_{Li} is the energy of an isolated free Li atom and E_H is the energy of a free hydrogen atom placed in a large cubic box. The effective number of atoms in the bulk unit cell is 2.

The calculated total energy of the H atom was found to be − 0.9522 Ry as indicated above was used to calculate the cohesive energy of LiH. The calculated cohesive energy was 6.784 eV. The experimental value was 9.40 ev (Chase, 1998). The deviation between the experimental value and the calculated value is 27.83%. Just like in the case of MgH_2, this energy is an indicator of the amount of energy that may be required for hydrogenation and dehydrogenation.

5.6 Formation Energy

Energy of formation is one of the most important quantities for hydrogen storage systems. The conditions of hydrogenation and dehydrogenation depend strongly on the energy of formation in the design of materials for hydrogen storage. Hydrogenation affects the host metal lattice and induces various effects such as lattice expansion and structural transformation (Miwa *et al.,* 2004). The energy of formation H_{form} may be decomposed into:

$$H_{form} = E_{transform} + E_{expansion} + E_{hydride}, \tag{5.5}$$

where $E_{transform}$, is the energy required to transform the host metal lattice into the arrangement of the metal ions in the metal hydride, $E_{expansion}$, is the energy required to expand the host metal lattice to that of the hydride and $E_{hydride}$, is the hydrogen insertion energy in the expanded metal lattice (Andreasen, 2001).

5.6.1 Formation Energy of MgH_2 and LiH

The reaction related to the formation of the hydride MgH_2 is:

$$Mg_{(s)} + H_{2(g)} \rightarrow MgH_{2(s)}. \tag{5.6}$$

Enthalpy of formation H_{form} (per hydrogen molecule) for MgH_2 is calculated as:

$$H_{form}(MgH_2) = E_{tot}(MgH_2) - E_{tot}(Mg) - E_{tot}(H_2), \tag{5.7}$$

where E_{tot} denotes the ground state total energy of compounds and reactants in their stable phases.

The ground state total energy of a hydrogen molecule was calculated as − 2.320 Ry, while other works reported a value of − 2.32 Ry (Nakamura *et al.,* 1998). The total energies were obtained with the optimized structures of MgH_2 and Mg. The enthalpy of formation is a measure of the stability of a compound. A positive enthalpy of formation denotes an unstable compound while a negative enthalpy of formation denotes a stable compound. Table 5.3 gives a comparison of calculated enthalpies for both MgH_2 and LiH with experimental values.

Table 5.3: Comparison of calculated enthalpies for MgH_2 and LiH.

Hydride	**H_{form} (kJ/mol.H_2)**	
	Calculated	**Experimental**
MgH_2	-78.20	-76.15 ±9.2 (Yamaguchi *et al.*, 1994)
LiH	-178.137	-116 (Grochala and Edwards, 2004)

From Table 5.3, the calculated enthalpy of formation of MgH_2 is − 78.20 kJ/mol.H_2. This value is in good agreement with the corresponding measured experimental value − 76.15 ± 9.2 kJ/mol. H_2 differing by only + 2.692%.

The enthalpy of formation for LiH was calculated using the same method. The

reaction related to the formation of LiH is:

$$Li_{(s)} + \frac{1}{2}H_{2(g)} \rightarrow LiH_{(s)}. \tag{5.8}$$

Enthalpy of formation H_{form} (per hydrogen molecule) for LiH is calculated as:

$$H_{form}(LiH) = E_{tot}(LiH) - E_{tot}(Li) - E_{tot}(H). \tag{5.9}$$

The total energies were obtained with the optimized structures of LiH and Li. Table 5.3 gives the enthalpy of formation of LiH as − 178.137 kJ/mol.H_2, a value that is rather different from the experimental one. The discrepancy could be attributed to the zero-point energy due to the vibration motion. Calculating the reaction enthalpies from the total energy differences neglects the contribution from atomic vibrations. Such contributions are negligible for heavy elements such as magnesium, whereas they may be significant for light elements like hydrogen and lithium (Miwa *et al.,* 2004).

Apart from having a high gravimetric hydrogen density, an ideal hydrogen storage material should also have moderate stability, that is, the ability to release hydrogen in an ambient temperature range. Formation energy is a very important aspect because in the design of hydrogen storage materials, the formation energy of these materials is expected to be stable at room temperature which means that the hydride can decompose at low temperature to release hydrogen. It is therefore paramount to note that formation energy determines the general operating temperature and pressure of a hydride compound, and if this value is beyond a particular range, it will be either too stable or too unstable for practical storage purposes.

According to Buschow *et al.,* (2000) the enthalpy of hydride formation can range from − 225 to + 52 kJ mol^{-1} for the binary hydrides (hydrogen absorption can be both endothermic and exothermic). The formation energy of magnesium hydride is consistent with its containing covalent bonds and having an intermediate character between ionic and covalent bonding as discussed under the density of states section.

However, the magnitude of the enthalpy is relatively high at – 78.2 kJ mol^{-1} H_2, resulting in a temperature of 545 K which is still too high compared with the ideal – 40 kJ mol^{-1} H_2, needed for a corresponding temperature of only 300 K. This therefore means that maintaining a magnesium hydride store at 550–600 K is inefficient since there are significant technological implications such as heat management during hydriding and dehydriding.

The high heat of formation of Magnesium Hydride is a major drawback to using the material for hydrogen storage due to the high operating temperatures required. This can however be dealt with by weakening the bonds between Magnesium and Hydrogen through processes such as ball milling, alloying with other transition metals and their oxides, catalysis and by use of intermetallic compounds.

5.7 Thermodynamic Properties

This section gives results of the first principle calculations of the thermodynamical properties of Magnesium Hydride and Lithium Hydride over a temperature range of 0–1000 K. The phonon dispersions determined were used to calculate the free energy of the two metal hydrides within the quasi harmonic approximation (QHA) at each temperature T.

5.7.1 Thermodynamic Properties of LiH

This section begins by giving the calculated thermodynamic properties of LiH, while those of MgH_2 will be discussed in subsequent sections. The concept of phonons has been used to determine the thermodynamic properties of different materials, and in this case, LiH. The phonon contribution to the Helmholtz free energy (ΔF), the internal energy (ΔE), the entropy (ΔS), and the heat capacity at constant volume (C_v) have been considered in this study. All the calculations were carried out using the QHA (Quasi Harmonic Approximation) code (Baroni *et al.,* 2011), where the thermodynamic properties of LiH were calculated over a temperature range of 0–1000 K. The phonon dispersions determined were used to calculate the free energy

of LiH within the quasi harmonic approximation (QHA) at each temperature T. The free energies were used to calculate various thermodynamical properties within QHA including the internal energy E, entropy S, and specific heat capacity at constant volume (C_v).

Table B. 1 in appendix B shows the calculated heat capacity at constant volume (C_v), the phonon contribution to entropy (ΔS), Helmholtz free energy (ΔF), the internal energy (ΔE), and corresponding experimental data at some selected temperatures from 0 to 1000 K for LiH. Since there are no documented experimental values of C_v for LiH, the experimental values of heat capacity at constant pressure (C_p) are used for comparison purposes, since $C_p = C_v - R$ (Gaskell, 2008).

Table B. 1 gives the calculated thermodynamic properties for LiH compared with experimental values where available. The temperature is in Kelvin while the values for S and C_p or C_v are in J/mol/K.

5.7.1.1 Entropy (S)

The temperature dependence of the entropy is (Gaskell, 2008),

$$\frac{\delta S(T,V)}{\delta T} = \left(\frac{\delta S}{\delta T}\right)_V + \left(\frac{\delta S}{\delta V}\right)_T \frac{\delta V}{\delta T}. \tag{5.10}$$

This contains harmonic, quasi harmonic, and anharmonic contributions, along with non harmonic effects from electron–phonon interactions. For LiH, calculated ΔS values are underestimated compared to the experimental values, but the consistency between the theoretical and the experimental data changes when the temperature is increased by every 25 K. The slightly larger error at higher temperature starting from 100 K suggests the limitation of the harmonic approximation, as it accounts only partially for the effects of anharmonicity. This is because the quasi harmonic model assumes that phonons are eigenstates of a phonon Hamiltonian for the expanded volume of the crystal, and it does not predict any shortening of phonon lifetimes. This is less appropriate at higher temperatures, where contribu-

tions to the potential energy is needed to understand the reduced phonon lifetimes, and shifts with temperature that may not depend quasi harmonically on the volume of the crystal and its bulk modulus (Fultz, 2010). To improve the theoretical results, a denser mesh is needed, but that means a huge computational task, or better pseudopotential approach should be used. The entropy as a function of temperature is an important thermodynamic quantity in thermodynamic modelling. It can be clearly seen that the entropy of LiH increases with temperature. Overall, the slight deviation between calculated and experimental data in entropy confirms that the theoretical considerations are reasonable. Figure 5.11 shows a comparison plot of the calculated phonon contribution to the entropy (S) and for LiH experiment values.

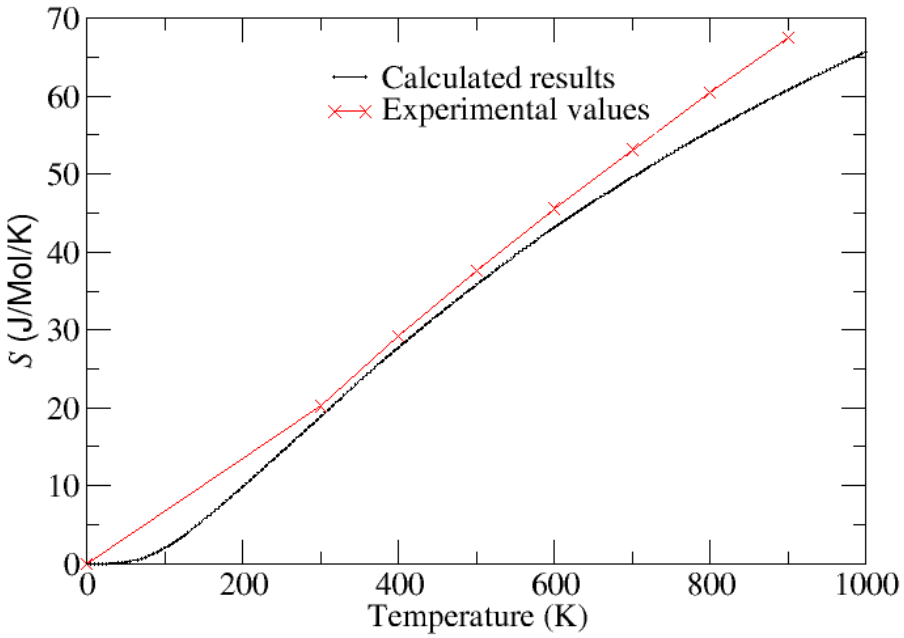

Figure 5.11: Calculated phonon contribution to the entropy (S) for LiH compared to experiment.

5.7.1.2 Specific Heat at Constant Volume (C_v)

Figure 5.12 shows the calculated phonon contribution to the heat capacity at constant volume C_v for LiH compared with experimental heat capacity at constant pressure C_p. Since $C_v \approx C_p$ for a solid, calculated values of C_v are compared directly with the experimental values of C_p. The relation between C_p and C_v can be given by the following equation:

$$C_p - C_v = \alpha^2 V(T) B_{(0)} T, \tag{5.11}$$

where α is the volume thermal expansion coefficient, B_0 is the bulk modulus, V is the volume and T is absolute temperature. According to this equation, the difference between C_p and C_v increases with increasing T, assuming other factors are independent of temperature. The difference between the C_p and C_v is not significant at low-temperature limit. However, at high temperatures C_v becomes smaller than C_p as seen from the plot. This implies that at low temperature limit, that is, as $T \rightarrow 0$ K, the specific heat C_v is determined from the vibrations of the low frequencies as well as electrons. As shown in Figure 5.12, C_v exhibits the T^3 power-law behaviour expected at the low-temperature limit, while at high temperatures the classical asymptotic limit of $C_V = 3nNkB \approx 50$ J/mol K is approached. This suggests that the calculated results can indeed be very useful as a prediction tool for future investigations within the limits of the temperatures that have been achieved in this work.

5.7.1.3 Internal Energy (E)

Figure 5.13 shows the calculated phonon contribution to the internal energy E for LiH. No experimental data exist for comparison but from the plot, a general trend is seen in which as the temperature increases, there is an increase in the internal energy. This parameter is important for the design of the hydrogen storage systems since in combination with other thermodynamic properties it can give an idea of

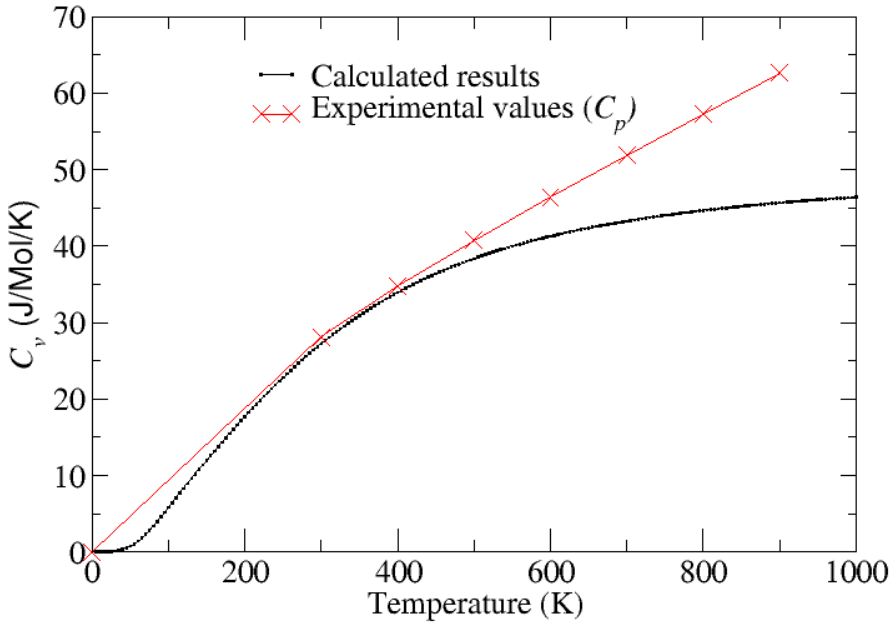

Figure 5.12: Calculated phonon contribution to the heat capacity at constant volume C_v for LiH compared with experimental heat capacity at constant pressure C_p.

just how much of the energy is required to charge and discharge the metal hydride. For LiH, the main objective is dehydriding and rehydriding of the metal hydride, which is infact charging and discharging of the metal hydride.

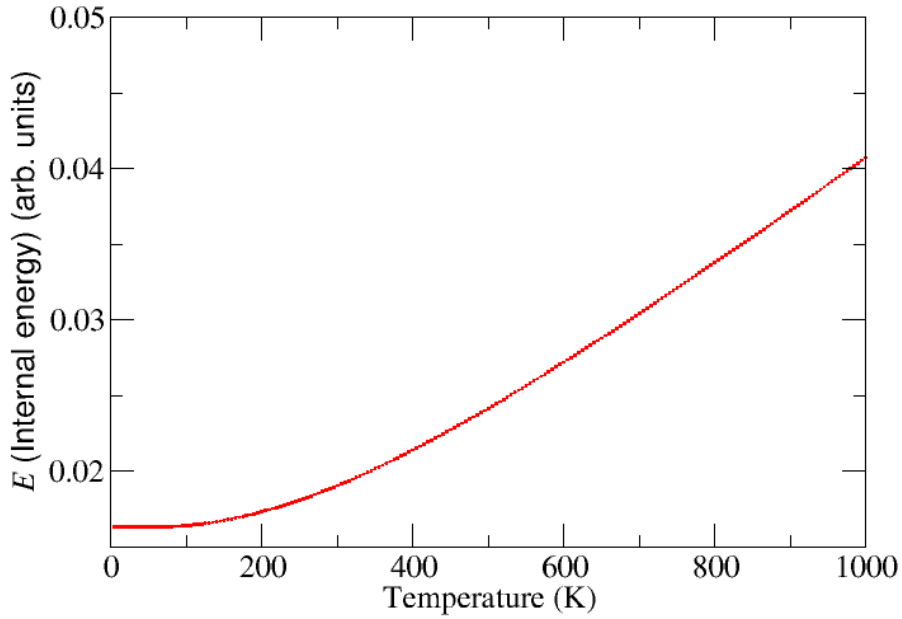

Figure 5.13: Calculated phonon contribution to the internal energy E for LiH.

5.7.1.4 Vibrational Energy (F)

Figure 5.14 shows the calculated phonon contribution to the Helmholtz free energy (F) for LiH. It also shows the temperature dependence of the Helmholtz free energy at a constant volume.

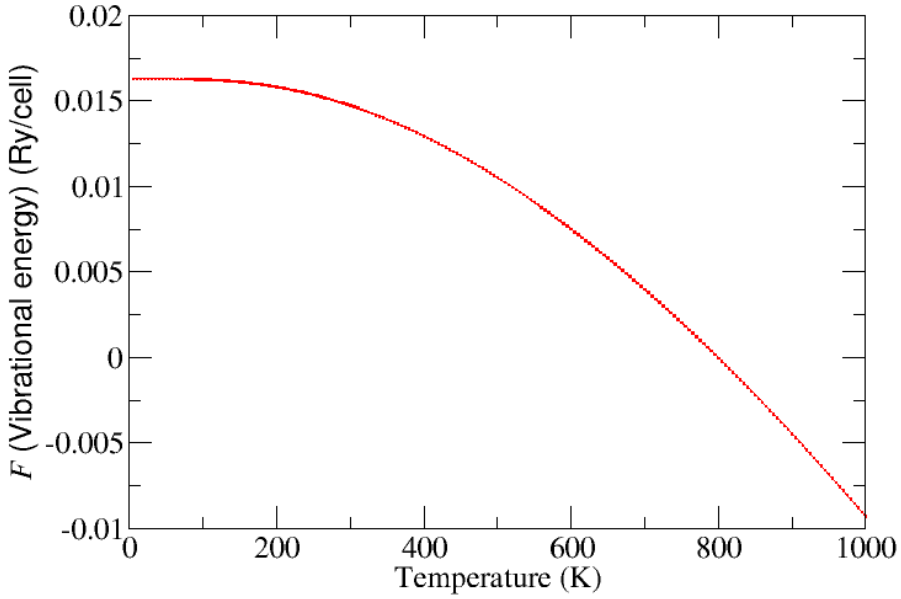

Figure 5.14: Calculated phonon contribution to the Helmholtz free energy (F) for LiH.

From Figure 5.14, it can be seen that as temperature increases, $F(V,T)$ decreases. This can be explained by rearranging the general formula for internal energy which is: Internal energy,

$$\triangle E = \triangle F + T\triangle S, \tag{5.12}$$

where E is the internal energy, F is the Helmholtz free energy, T is the temperature and S is the entropy. To obtain the Helmholtz free energy, the equation is rearranged to be:

$$F = E–TS. \tag{5.13}$$

It can then be clearly seen from Figure 5.14 that both E and TS increase with temperature. The slope of the curve for TS is greater than that of E. However, the

rise in TS is more, so as to be able to compensate for the rise in E. Hence, $F(V,T)$ decreases with increase in temperature as exhibited in Figure 5.14.

It is important to mention that the thermodynamic properties of a storage material govern its operating temperature and pressure range. As such, these must be considered in conjunction with the reversible storage capacity and the kinetics of hydrogen sorption properties of a material. These form a fundamental measure of the hydrogen storage properties of a particular host, whether an adsorbent or an absorber.

5.7.2 Thermodynamic Properties of MgH_2

As in the case for LiH, the same concept of phonons was used to determine the thermodynamic properties of MgH_2. The properties that were determined include the phonon contribution to the Helmholtz free energy (ΔF), the internal energy (ΔE), the entropy (ΔS), and the heat capacity at constant volume C_v. All the calculations were carried out using the QHA (Quasi Harmonic Approximation) code. Thermodynamic properties of MgH_2 were calculated over a temperature range of 0–1000 K. The phonon dispersions were determined within the density functional framework and were used to calculate the free energy of MgH_2 within the quasi harmonic approximation (QHA) at each temperature T. Table B. 2 in the appendix section shows the calculated heat capacity at constant volume C_v, the phonon contribution to entropy (ΔS), Helmholtz free energy (ΔF), the internal energy (ΔE), and corresponding experimental data at selected temperatures from 0 to 1000 K for MgH_2. Since there are no documented experimental values of C_v, the experimental values of heat capacity at constant pressure (C_p) were used for comparison purposes.

5.7.2.1 Entropy (S)

A plot of temperature against entropy for MgH_2 showed that the calculated ΔS values were somewhat underestimated compared to the experimental ones. However, no experimental data exists for comparison purposes for the temperature of 0 to 299

K. Experimental values available for comparison exist from a temperature of 300 to 600 K for one reference and another one within the same range of temperature. At a temperature of 300 K, the calculated value of this present work was found to be underestimated by about -0.126% to the experimental values. At a temperature of 500 K, the calculated value was underestimated by about -3.42%, while at 700 K, the calculated value of entropy was underestimated by about -4.52%. This parameter was underestimated by about -5.95% from the experimental data at 1000 K.

From this trend, it can be seen that the agreement between the experimental and calculated values in terms of deviation is small at lower temperatures but as the temperature increases, the deviation increases. This can be clearly seen from Figure 5.15 which shows a plot of the calculated phonon contribution to the entropy (S) for MgH_2 compared to experiment. The larger deviation at higher temperatures can be attributed to the limitation of the harmonic approximation, as it accounts only partially for the effects of anharmonicity as pointed out earlier. This is less appropriate at higher temperatures where the potential energies are needed to understand the reduced phonon life times, and shifts with temperature that may not depend quasi harmonically on the volume of the crystal and its bulk modulus (Fultz, 2010). It can be attributed to the fact that that Quasi Harmonic Approximation (Q.H.A) is known to work at temperatures below the melting point of a system under study.

In this work, calculations were performed at temperatures below and beyond 573 K. This was done to access the level of agreement between the QHA results at high temperatures with the experimental values. However, the temperature dependence of entropy was found to be in reasonable agreement with the experimental results thereby exhibiting QHA as a good theoretical approach for calculating these quantities even at temperatures greater than the melting point of MgH_2 (573K).

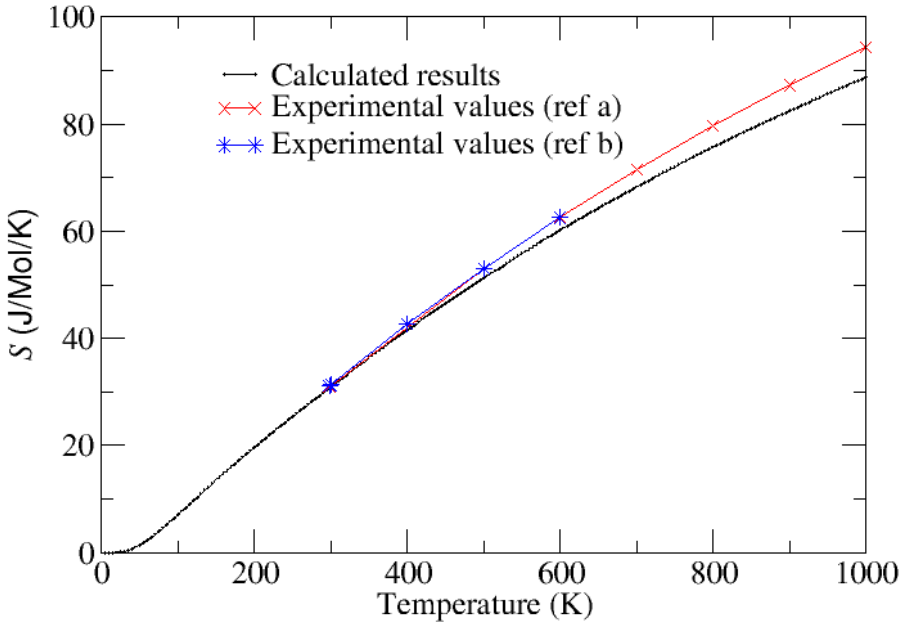

Figure 5.15: Calculated phonon contribution to the entropy (S) for MgH_2 compared to experiment.

[a] (Chase, 1998), [b] (Ihsan, 2006).

5.7.2.2 Specific Heat at Constant Volume (C_v)

Figure 5.16 shows the calculated phonon contribution to the heat capacity at constant volume, C_v, for MgH_2 compared with experimental heat capacity at constant pressure, C_p.

Experimental data available is for C_p, but since $C_v \approx C_p$ for a solid, calculated values C_v are compared directly with the experimental values of C_p. From Figure 5.16, the difference between the C_p and C_v is not significant at low temperatures of up to 250 K. At high temperatures, values of C_v are smaller than C_p. This can be attributed to the determination of C_v is from the vibrations of the low frequencies. The temperature dependence of C_v was found to be in reasonable agreement with the experimental results thereby exhibiting QHA as a reliable theoretical approach for calculating these quantities even at temperatures greater than the melting point of MgH_2.

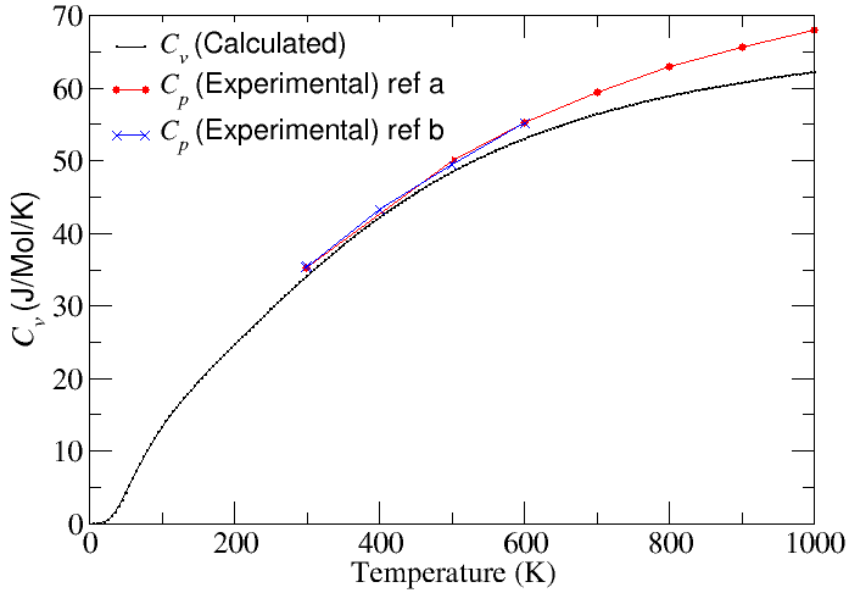

Figure 5.16: Calculated phonon contribution to the heat capacity at constant volume C_v for MgH_2 compared with experimental heat capacity at constant pressure C_p.

[a] (Chase, 1998), [b] (Ihsan, 2006).

5.7.2.3 Internal Energy (E)

The suitability of metal hydride systems for hydrogen storage and other applications is closely related to their thermodynamic properties. Figure 5.17 shows the calculated phonon contribution to the internal energy (E) for MgH_2. However, no experimental data exist for comparison but from the plot, a general trend is seen in which as the temperature increases, there is an increase in the internal energy. The internal energy is important for the design of the hydrogen storage systems, since for every hydrogen storage medium, just like for the case of LiH mentioned earlier, the target is dehydriding and rehydriding of the metal hydride, which in effect is the charging and discharging the metal hydride. A change in the internal energy, in combination with other thermodynamic properties can give an idea of just how much energy is required to charge and discharge the metal hydride.

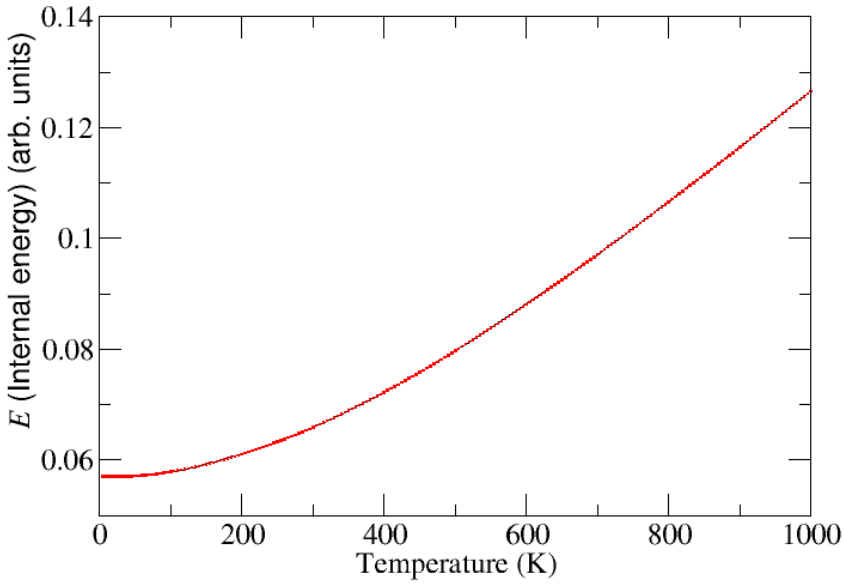

Figure 5.17: Calculated phonon contribution to the internal energy E for MgH_2.

5.7.2.4 Vibrational Energy (F)

Figure 5.18 shows the calculated phonon contribution to the Helmholtz free energy (F) for MgH_2. From Figure 5.18, it can be seen that as temperature increases, $F(V,T)$ decreases in a non-linear manner. This can be explained by the reasons given earlier under the LiH section on vibrational energy, that, whenever the temperature increases, the term TS in equation 5.12 increases, thereby lowering the numerical value of energy F. Although the internal energy (E) is a function of temperature (T), that is, $E = E(T)$, its increment is much smaller compared to that of the TS term, and hence the Helmholtz free energy (F) generally decreases with increase in temperature.

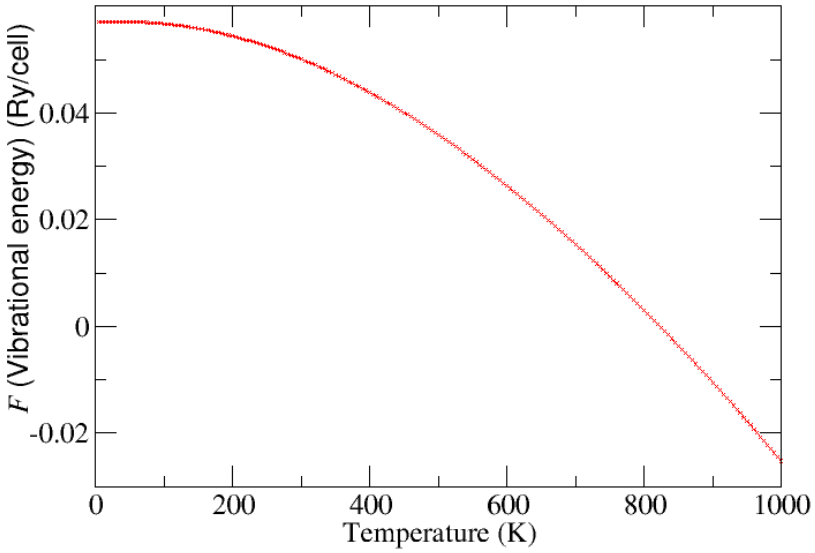

Figure 5.18: Calculated phonon contribution to the Helmholtz free energy (F) for MgH_2.

CHAPTER SIX

CONCLUSIONS AND RECOMMENDATIONS

6.1 Conclusions

This study has considered the two most promising candidates for use in solid state hydrogen storage, that is, MgH_2 and LiH. The calculated structural properties showed agreement with the experimental values. A lattice constant of $a = 4.540$ Å, $b = 4.540$ Å and $c = 3.019$ Å was obtained for MgH_2, which differed only slightly with the experimental value of $a = b = 4.501$ Å and $c = 3.01$ Å (Noritake *et al.,* 2003). For LiH, the calculated lattice constants were $a = b = c = 3.93$ Å. Thus, a comparison of the calculated lattice constant for MgH_2 and LiH with experimental findings showed that these differed only marginally from experiment by +0.8% and -3.7%, respectively. The bulk modulus of MgH_2 was 56.85 GPa while that of LiH was 39.90 GPa. No experimental data exists for the bulk modulus of MgH_2 for comparison to the best of my knowledge, and hence this study is an important guide to future experimental works on MgH_2.

Electronic structure calculations confirmed that both LiH and MgH_2 were both insulators, whereby LiH had a wide direct electronic band gap of 3.0 eV. MgH_2 is also an insulator with a wide indirect electronic band gap of 3.65 eV. PDOS of MgH_2 revealed that there was presence of H-1s and Mg-3p states which had some amount of covalent H–H contribution to the bonding. PDOS for LiH showed some contribution from the 1s orbital of H as well as 1s and 2p orbitals of Li, which were indicative of hybridization during bonding of the crystal. LiH was found to posses both ionic bonds and covalent character in the bonds.

The formation energy of MgH_2 was found to be –78.2 kJ mol^{-1} H_2 while that of LiH was −178.137 kJ/mol.H_2. The experimental value for formation energy of MgH_2 is -76.15 ±9.2 kJ mol^{-1} H_2 (Yamaguchi *et al.*, 1994) while that of LiH is -116 kJ mol^{-1} H_2 (Grochala and Edwards, 2004). The heats of formation therefore suggest that the two metal hydrides are suitable for hydrogen storage applications. The study

revealed that the trend observed in experimental studies is followed, whereby MgH_2 has a lower formation energy than LiH, although both the calculated values were slightly different from the corresponding experimental values. This can, however, be explained from the assumptions made in the theoretical modelling.

Calculated thermodynamic properties for both LiH and MgH_2 were in good agreement with experimental data. In particular, at all temperatures, the calculated entropies matched to within 4.5% of the literature values. The predicted heat capacities at 500 and 600 K showed a deviation of 4.1% and 3.5% from the corresponding reference values. At other temperatures, the proximity between the calculated and experimental values was always within 2.5%. Thus, Quasi Harmonic Approximation can be used as a tool for computing the thermodynamical properties of both LiH and MgH_2 to a reasonable degree of accuracy at low, as well as high temperatures and hence predicting their stability for use in hydrogen fuel storage applications.

6.2 Recommendations for Future Work

This work dealt with some of the properties required to modify the metal hydrides to enhance their hydrogen storage ability. There is need for more research into ways of decreasing the stability of the metal hydrides to be done computationally before it can be put into practice experimentally. This is because computational methods support experimental work and are reasonably predictive, where data is not available.

There is also need to study more on the surface properties of the two metal hydrides. This is because when hydrogen is desorbed from the bulk material, it must go through the surface and thus surface calculations are also of paramount importance for understanding the whole process in great detail.

REFERENCES

Andreasen, A. (2001). Predicting formation enthalpies of metal hydrides. *Nature*, **414,** 353 - 358.

Ayers, P. W., Golden, S., and Levy, M. (2006). Generalizations of the Hohenberg-Kohn theorem: I. Legendre transform constructions of variational principles for density matrices and electron distribution functions. *The Journal of Chemical Physics,* **124**, 054101.

Ball, M., and Wietschel, M. (2009). *The hydrogen economy: opportunities and challenges.* Cambridge University Press.

Barbir, F., and Gomez, T. (1997). Efficiency and economics of proton exchange membrane (PEM) fuel cells. *International Journal of Hydrogen Energy,* **22** (10), 1027-1037.

Baroni, S., Giannozzi, P., and Isaev, E. (2011). Thermal properties of materials from *ab-initio* quasi-harmonic phonons. *arXiv preprint arXiv*:1112.4977.

Blaha, P., Hofstätter, H., Koch, O., Laskowski, R., and Schwarz, K. (2010). Iterative diagonalization in augmented plane wave based methods in electronic structure calculations. *Journal of Computational Physics,* **229** (2), 453-460.

Bloch, J., and Mintz, M. H. (1997). Kinetics and mechanisms of metal hydrides formation—a review. *Journal of Alloys and Compounds,* **253**, 529-541.

Bobet, J. L., Akiba, E., Nakamura, Y., and Darriet, B. (2000). Study of Mg-M (M= Co, Ni and Fe) mixture elaborated by reactive mechanical alloying—hydrogen sorption properties. *International Journal of Hydrogen Energy*, **25** (10), 987-996.

Bortz, M., Bertheville, B., Böttger, G., and Yvon, K. (1999). Structure of the high pressure phase γ-MgH_2 by neutron powder diffraction. *Journal of Alloys and Compounds*, **287** (1), L4-L6.

Bouhadda, Y., Rabehi, A., and Bezzari-Tahar-Chaouche, S. (2007). First-principle calculations of MgH_2 and LiH for hydrogen storage. *Revue des Energies Renouvelables*, **10** (4), 545-550.

Brika, M. G., and Kityk, I. V. (2011). *ab-initio* analysis of the optical, electronic and elastic properties of the hydrogen-storage single crystals $LiNH_2$. *Materials Chemistry and Physics* **130**: 685– 689.

Budd, P. M., Butler, A., Selbie, J., Mahmood, K., McKeown, N. B., Ghanem, B., and Walton, A. (2007). The potential of organic polymer-based hydrogen storage materials. *Physical Chemistry Chemical Physics*, **9** (15), 1802-1808.

Buschow, K. H. J., Bouten, P. C. P., and Miedema, A. R. (2000). Hydrides formed from intermetallic compounds of two transition metals: a special class of ternary alloys. *Reports on Progress in Physics*, **45** (9), 937.

Cazorla, C., and Boronat, J. (2005). Isotopic effects in solid LiH and LiD at very low temperature. *Journal of Low Temperature Physics*, **139** (5), 645-650.

Ceperley, D. M., and Alder, B. J. (1980). Ground state of the electron gas by a stochastic method. *Physical Review Letters*, **45** (7), 566-569.

Chadi, D. J., and Cohen, M. L. (1973). Special points in the Brillouin zone. *Physical Review B*, **8** (12), 5747.

Chase, M. W. (1998). *NIST-JANAF thermochemical tables.* 4^{th} Ed. vol. 9. New York: American Institute of Physics.

Chen, Y., and Williams, J. S. (1995). Formation of metal hydrides by mechanical alloying. *Journal of Alloys and Compounds*, **217** (2), 181-184.

Cheng, X., Shi, Z., Glass, N., Zhang, L., Zhang, J., Song, D., and Shen, J. (2007). A review of PEM hydrogen fuel cell contamination: Impacts, mechanisms, and mitigation. *Journal of Power Sources*, **165** (2), 739-756.

Cuevas, J. C., and Scheer, E. (2010). *Molecular electronics: an introduction to theory and experiment.* (Vol. 1). World Scientific.

David, E. (2005). An overview of advanced materials for hydrogen storage. *Journal of Materials Processing Technology*, **162**, 169-177.

Dehouche, Z., Klassen, T., Oelerich, W., Goyette, J., Bose, T. K., and Schulz, R. (2002). Cycling and thermal stability of nanostructured MgH_2–Cr_2O_3 composite for hydrogen storage. *Journal of Alloys and Compounds*, **347** (1), 319-323.

Dinh, L. N., Cecala, C. M., Leckey, J. H., and Balooch, M. (2001). The effects of moisture on LiD single crystals studied by temperature-programmed decomposition. *Journal of Nuclear Materials*, **295** (2), 193-204.

Dinh, L. N., Mclean Ii, W., Schildbach, M. A., LeMay, J. D., Siekhaus, W. J., and Balooch, M. (2003). The nature and effects of the thermal stability of lithium hydroxide. *Journal of Nuclear Materials*, **317** (2), 175-188.

Edwards, P. P., Kuznetsov, V. L., David, W. I. F. and Brandon, N. P. (2008). Hydrogen and fuel cells: Towards a sustainable energy future. *Energy Policy*, **36** (12), 4356–4362.

Einstein, A., and Hopf, L. (1910). On a theorem of the probability calculus and its application to the theory of radiation. *Annals of Physics*, **33**, 1096-1104.

Engel, E., and Dreizler, R. M. (2011). *Density Functional Theory: An Advanced Course.* Springer.

Evarestov, R. A., and Smirnov, V. P. (1983). Special points of the Brillouin zone and their use in the solid state theory. *Physica Status Solidi (b)*, **119** (1), 9-40.

Fultz, B. (2010). Vibrational thermodynamics of materials. *Progress in Materials Science*, **55** (4), 247-352.

Gaskell, D. (2008). *Introduction to the Thermodynamics of Materials*, 5^{th} Ed.,

Taylor and Francis.

Gennari, F. C., Castro, F. J., and Urretavizcaya, G. (2001). Hydrogen desorption behaviour from magnesium hydrides synthesized by reactive mechanical alloying. *Journal of Alloys and Compounds*, **321** (1), 46-53.

Gennari, F. C., Castro, F. J., Urretavizcaya, G., and Meyer, G. (2002). Catalytic effect of Ge on hydrogen desorption from MgH_2. *Journal of Alloys and Compounds*, **334** (1), 277-284.

Gerlich, D., and Smith, C. S. (1974). The pressure and temperature derivatives of the elastic moduli of lithium hydride. *Journal of Physics and Chemistry of Solids*, **35** (12), 1587-1592.

Giannozzi, P., Baroni, S., Bonini, N., Calandra, M., Car, R., Cavazzoni, C., and Wentzcovitch, R. M. (2009). QUANTUM ESPRESSO: a modular and open-source software project for quantum simulations of materials. *Journal of Physics: Condensed Matter*, **21** (39), 395502.

Grochala, W., and Edwards, P. P. (2004). Thermal decomposition of the non-interstitial hydrides for the storage and production of hydrogen. *Chemical Reviews-Columbus*, **104** (3), 1283-1316.

Guoxian, L., Erde, W., and Shoushi, F. (1995). Hydrogen absorption and desorption characteristics of mechanically milled Mg 35 wt.% $FeTi_{1.2}$ powders. *Journal of Alloys and Compounds*, **223** (1), 111-114.

Herbst, J. F., and Hector Jr, L. G. (2005). Energetics of the Li amide/Li imide hydrogen storage reaction. *Physical Review B*, **72** (12), 125120.

Holtz, R. L., and Imam, M. A. (1999). Hydrogen storage characteristics of ball-milled magnesium-nickel and magnesium-iron alloys. *Journal of Materials Science*, **34** (11), 2655-2663.

Hong, T. W., Kim, S. K., and Kim, Y. J. (2000). Dehydrogenation properties of

nano-amorphous Mg_2NiH_x by hydrogen induced mechanical alloying. *Journal of Alloys and Compounds*, **312** (1), 60-67.

Huot, J., Liang, G., and Schulz, R. (2001). Mechanically alloyed metal hydride systems. *Applied Physics A: Materials Science and Processing*, **72** (2), 187-195.

Ihsan, B. (2006). *Thermochemical Data of Pure substances.* New York: Wiley-VCH Verlag GmbH.

Joannopoulos, J. D., and Cohen, M. L. (1973). Electronic properties of complex crystalline and amorphous phases of Ge and Si. I. Density of states and band structures. *Physical Review B*, **7** (6), 2644.

Jones, R. O. and Gunnarsson, O. (1989). The density functional formalism, its applications and prospects. *Reviews of Modern Physics,* vol. **61**, p. 689.

Kanagaprabha, S., Asvini, A. T., and Iyakutti, K. (2012). First principles study of pressure induced structural phase transition in hydrogen material—MgH_2. *Physica B: Condensed Matter*, **407** (1), 54–59.

Kittel, C. (2005). *Introduction to Solid State Physics*, 8^{th} Ed.New York: John WILEY.

Klein, M. J. (1990). *The Physics of J. Willard GIBBS in his time.* CALDI and MOSTOW, pg. 1-21.

Koch, W. and Holthausen, M. C. (2001). *A Chemist's Guide to Density Functional Theory.* Wiley-VCH.

Kohn, W., and Sham, L. J. (1965). Self-consistent equations including exchange and correlation effects (pp. A1133-A1138). Defense Technical Information Center.

Kokalj, A. (2003). Computer graphics and graphical user interfaces as tools in simulations of matter at the atomic scale. *Computational Materials Science*, **28** (2), 155-168.

Kresse, G., and Furthmuller, J. (1996). Efficiency of *ab-initio* total energy calculations for metals and semiconductors using a plane-wave basis set. *Computational Materials Science*, **6** (1), 15-50.

Laasonen, K., Sprik, M., Parrinello, M., and Car, R. (1993). *"ab-initio"* liquid water. *The Journal of Chemical Physics*, **99**, 9080.

Langmi, H. W., Book, D., Walton, A., Johnson, S. R., Al-Mamouri, M. M., Speight, J. D., and Anderson, P. A. (2005). Hydrogen storage in ion-exchanged zeolites. *Journal of Alloys and Compounds*, **404**, 637-642.

Lee, B. K., Stout, J. M., and Dykstra, C. E. (1997). *ab-initio* calculations of lithium hydride. *Journal of Molecular Structure: THEOCHEM*, **400**, 57-68.

Liang, G., Boily, S., Huot, J., Van Neste, A., and Schulz, R. (1998). Mechanical alloying and hydrogen absorption properties of the Mg–Ni system. *Journal of Alloys and Compounds*, **267** (1), 302-306.

Lide, D. R. (2012). *CRC Handbook of Chemistry and Physics*. Boca Raton, FL: CRC press.

Lin, X., Jia, J., Zhao, X., Thomas, K. M., Blake, A. J., Walker, G. S., and Schröder, M. (2006). High H_2 Adsorption by Coordination -Framework Materials. *Angew and teChemie International Edition*, **45** (44), 7358-7364.

Loubeyre, P., Le Toullec, R., Hanfland, M., Ulivi, L., Datchi, F., and Hausermann, D. (1998). Equation of state of ^{7}LiH and ^{7}LiD from X-ray diffraction to 94 GPa. *Physical Review B*, **57** (17), 10403.

Manchester, F. D., and Khatamian, D. (2008). Mechanisms for activation of intermetallic hydrogen absorbers. *In Materials Science Forum* (Vol. **31**, pp. 261-296).

Maradudin, A. A. (1971). *Theory of lattice dynamics in the harmonic approximation*. 2^{nd} Ed. New York: Academic press.

Mayer, I. (2003). *Simple theorems, proofs and derivations in quantum chemistry.* Springer.

Miwa, K., Ohba, N., Towata, S. I., Nakamori, Y., and Orimo, S. I. (2004). First-principles study on lithium borohydride $LiBH_4$. *Physical Review B*, **69** (24), 245120.

Monkhorst, H. J., and Pack, J. D. (1976). Special points for Brillouin-zone integrations. *Physical Review B*, **13** (12), 5188-5192.

Montone, A., VittoriAntisari, M., Abazović, N., GrbovićNovaković, J., Pasquini, L., Bonetti, E., and Fiorini, A. L. (2007). Reaction with hydrogen of micro and nano composites based on Mg. *In Materials Science Forum* (Vol. **555**, pp. 335-342).

Moyses, C. A., Lebegue, S., Eriksson, O., Arnaud, B., Alouani, M., and Ahuja, R. (2005). Electronic and optical properties of α, γ, and β phases of MgH_2: A first-principles GW investigation. *Journal of Applied Physics*, **98** (9), 096106-096106.

Nakamura, H., Nguyen-Manh, D., and Pettifor, D. G. (1998). Electronic structure and energetics of $LaNi_5$, α-$La_2Ni_{10}H$ and β-$La_2Ni_{10}H_{14}$. *Journal of Alloys and Compounds*, **281** (2), 81-91.

Noritake, T., Towata, S., Aoki, M., Seno, Y., Hirose, Y., Nishibori, E., and Sakata, M. (2003). Charge density measurement in MgH_2 by synchrotron X-ray diffraction. *Journal of Alloys and Compounds*, **356**, 84-86.

Novakovi, N., Radisavljević, I., Colognesi, D., Ostojić, S., and Ivanović, N. (2007). First principle calculations of alkali hydride electronic structures. *Journal of Physics: Condensed Matter*, **19** (40), 406211.

Novaković, N., Matović, L., Novaković, J. G., Manasijević, M., and Ivanović, N. (2009). *ab-initio* study of MgH_2 formation. *Materials Science and Engineering*: B, **165** (3), 235-238.

Oelerich, W., Klassen, T., and Bormann, R. (2001). Metal oxides as catalysts for improved hydrogen sorption in nanocrystalline Mg-based materials. *Journal of*

Alloys and Compounds, **315** (1), 237-242.

Oxtoby, D. W., Gillis, H. P., and Campion, A. (2007). *Principles of Modern Chemistry*, 6 th Ed. Belmont, USA: Brooks/Cole.

Payne, M. C., Teter, M. P., Allan, D. C., Arias, T. A., and Joannopoulos, J. D. (1992). Iterative minimization techniques for *ab-initio* total-energy calculations: molecular dynamics and conjugate gradients. *Reviews of Modern Physics*, **64** (4), 1045-1097.

Perdew, J. P., and Zunger, A. (1981). Self-interaction correction to density-functional approximations for many-electron systems. *Physical Review B*, **23** (10), 5048.

Perdew, J. P., Burke, K., and Ernzerhof, M. (1998). Perdew, Burke, and Ernzerhof Reply. *Physical Review Letters*, **80** (4), 891-891.

Perdew, J. P., Chevary, J. A., Vosko, S. H., Jackson, K. A., Pederson, M. R., Singh, D. J., and Fiolhais, C. (1992). Atoms, molecules, solids, and surfaces: Applications of the generalized gradient approximation for exchange and correlation. *Physical Review B*, **46** (11), 6671.

Pozzo, M. and Alfè D. (2008). Structural properties and enthalpy of formation of magnesium hydride from quantum Monte Carlo calculations. *Physical Review B*, **77**: 104103.

Principi, G., Agresti, F., Maddalena, A., and Lo Russo, S. (2009). The problem of solid state hydrogen storage. *Energy*, **34** (12), 2087-2091.

Sakintuna, B., Lamari-Darkrim, F., and Hirscher, M. (2007). Metal hydride materials for solid hydrogen storage: a review. *International Journal of Hydrogen Energy*, **32** (9), 1121-1140.

Sato, T., Kyoi, D., Rönnebro, E., Kitamura, N., Sakai, T., and Noréus, D. (2006). Structural investigations of two new ternary magnesium–niobium hydrides, $Mg_{6.5}NbH_{14}$ and $MgNb_2H_4$. *Journal of Alloys and Compounds*, **417** (1), 230-234.

Scheiner, A. C., Baker, J., and Andzelm, J. W. (1998). Molecular energies and properties from density functional theory: Exploring basis set dependence of Kohn—Sham equation using several density functionals. *Journal of Computational Chemistry*, **18** (6), 775-795.

Schlapbach, L., and Züttel, A. (2001). Hydrogen-storage materials for mobile applications. *Nature*, **414** (6861), 353-358.

Schuth, F., Bogdanović, B., and Felderhoff, M. (2004). Light metal hydrides and complex hydrides for hydrogen storage. *Chemical Communications*, **(20)**, 2249-2258.

Sherif, S. A., Zeytinoglu, N., and Veziroğlu, T. N. (1997). Liquid hydrogen: potential, problems, and a proposed research program. *International Journal of Hydrogen Energy*, **22** (7), 683-688.

Sholl, D., and Steckel, J. A. (2011). *Density functional theory: a practical introduction.* Wiley. com.

Smithson, H., Marianetti, C. A., Morgan, D., Van der Ven, A., Predith, A., and Ceder, G. (2002). First-principles study of the stability and electronic structure of metal hydrides. *Physical Review B*, **66** (14), 144107.

Soloveichik, G. L. (2007). Metal borohydrides as hydrogen storage materials. *Material Matters*, **2**, 11-4.

Takeichi, N., Senoh, H., Yokota, T., Tsuruta, H., Hamada, K., Takeshita, H. T., and Kuriyama, N. (2003). "Hybrid hydrogen storage vessel", a novel high-pressure hydrogen storage vessel combined with hydrogen storage material. *International Journal of Hydrogen Energy*, **28** (10), 1121-1129.

Thijssen, J. (2007). *Computational physics.* Cambridge University Press.

Troullier, N., and Martins, J. L. (1991). Efficient pseudopotentials for plane-wave calculations. *Physical Review B*, **43** (3), 1993.

Tyuterev, V. G., and Vast, N. (2006). Murnaghan's equation of state for the electronic ground state energy. *Computational Materials Science*, **38** (2), 350-353.

Van Setten, M. J., Popa, V. A., De Wijs, G. A., and Brocks, G. (2007). Electronic structure and optical properties of lightweight metal hydrides. *Physical Review B*, **75** (3), 035204.

Vanderbilt, D. (1990). Soft self-consistent pseudo potentials in a generalized eigenvalue formalism. *Physical Review B*, **41** (11), 7892.

Varin, R. A., Czujko, T., and Wronski, Z. S. (2008). *Nanomaterials for Solid State Hydrogen Storage*. New York: Springer.

Wagemans, R. W., van Lenthe, J. H., de Jongh, P. E., Van Dillen, A. J., and de Jong, K. P. (2005). Hydrogen storage in magnesium clusters: quantum chemical study. *Journal of the American Chemical Society*, **127** (47), 16675-16680.

Walker, G. (Ed.). (2008). *Solid-State Hydrogen Storage: Materials and Chemistry*. Woodhead Publishing.

Wang, H. Y., Xu, H., Huang, T. T., and Deng, C. S. (2008). Thermodynamics of wurtzite GaN from first-principle calculations. *The European Physical Journal B-Condensed Matter and Complex Systems*, **62** (1), 39-43.

Wu, Z., Allendorf, M. D., and Grossman, J. C. (2009). Quantum Monte Carlo Simulation of Nanoscale MgH_2 Cluster Thermodynamics. *Journal of the American Chemical Society*, **131** (39), 13918-13919.

Xia, Z. T., and Chan, S. H. (2005). Feasibility study of hydrogen generation from sodium borohydride solution for micro fuel cell applications. *Journal of Power Sources*, **152**, 46-49.

Yamaguchi, M., Akiba, E., Cahn, R. W., Haasen, P., and Kramer, E. J. (1994). *Materials Science and Technology*, Vol. **3B**. New York: VCH, pp 333-345.

Yang, Z., Xia, Y., and Mokaya, R. (2007). Enhanced hydrogen storage capacity of high surface area zeolite-like carbon materials. *Journal of the American Chemical Society*, **129** (6), 1673-1679.

Yu, R., and Lam, P. K. (1988). Electronic and structural properties of MgH_2. *Physical Review B*, **37**(15), 8730.

Zaluska, A., and Zaluski, L. (2005). New catalytic complexes for metal hydride systems. *Journal of Alloys and Compounds*, **404**, 706-711.

Zaluska, A., Zaluski, L., and Ström–Olsen, J. O. (1999). Nanocrystalline magnesium for hydrogen storage. *Journal of Alloys and Compounds*, **288** (1), 217-225.

Zaluski, L., Zaluska, A., Tessier, P., Ström-Olsen, J. O., and Schulz, R. (1995). Catalytic effect of Pd on hydrogen absorption in mechanically alloyed Mg_2Ni, $LaNi_5$ and FeTi. *Journal of Alloys and Compounds*, **217** (2), 295-300.

Zhang, H. F., Yu, Y., Zhao, Y. N., Xue, W. H., and Gao, T. (2010). *ab-initio* electronic, dynamic, and thermodynamic properties of isotopic lithium hydrides ^{6}LiH, ^{6}LiD, ^{6}LiT, ^{7}LiH, ^{7}LiD, and ^{7}LiT. *Journal of Physics and Chemistry of Solids*, **71** (7), 976-982.

Zhu, M., Wang, H., Ouyang, L. Z., and Zeng, M. Q. (2006). Composite structure and hydrogen storage properties in Mg-base alloys. *International Journal of Hydrogen Energy*, **31** (2), 251-257.

Zuttel, A. (2003). Materials for hydrogen storage. *Materials Today*, **6** (9), 24-33.

Zuttel, A. (2004). Hydrogen storage methods. *Naturwissenschaften*, **91**, 157-172.

APPENDIX A

k-POINTS AND CUT OFF ENERGY OPTIMIZATION

Figure A. 1 shows the optimization plot of k-points for Mg.

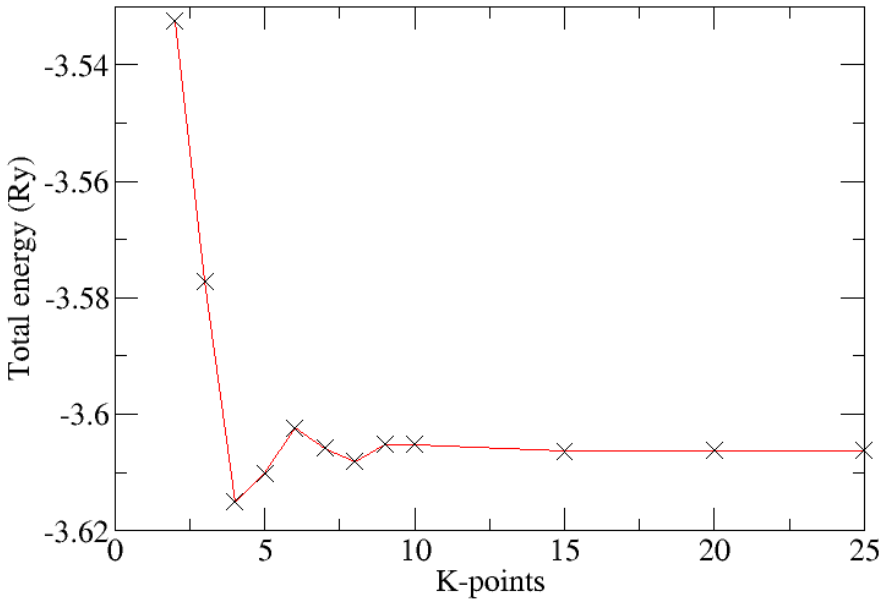

Figure A.1: A plot of k-points convergence of Mg.

A converged k-point mesh of 10×10×10 was considered for Mg since it had the lowest energy for the structure and had a consistent energy. A k-point mesh of

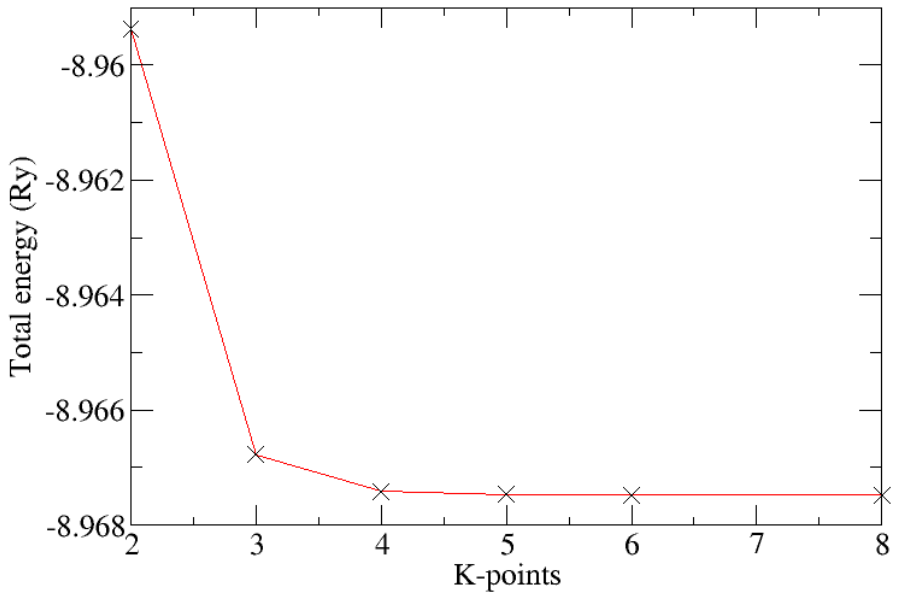

Figure A.2: A plot of k points convergence of MgH_2.

4×4×6 was taken for MgH_2 since it had the lowest energy for the structure.

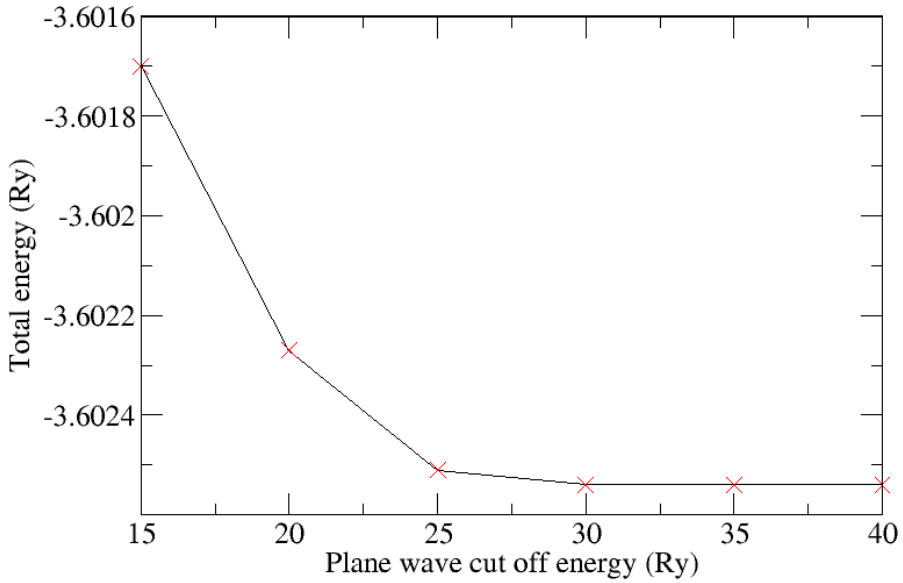

Figure A.3: A plot of the total energy for Mg versus the plane wave cut off energy.

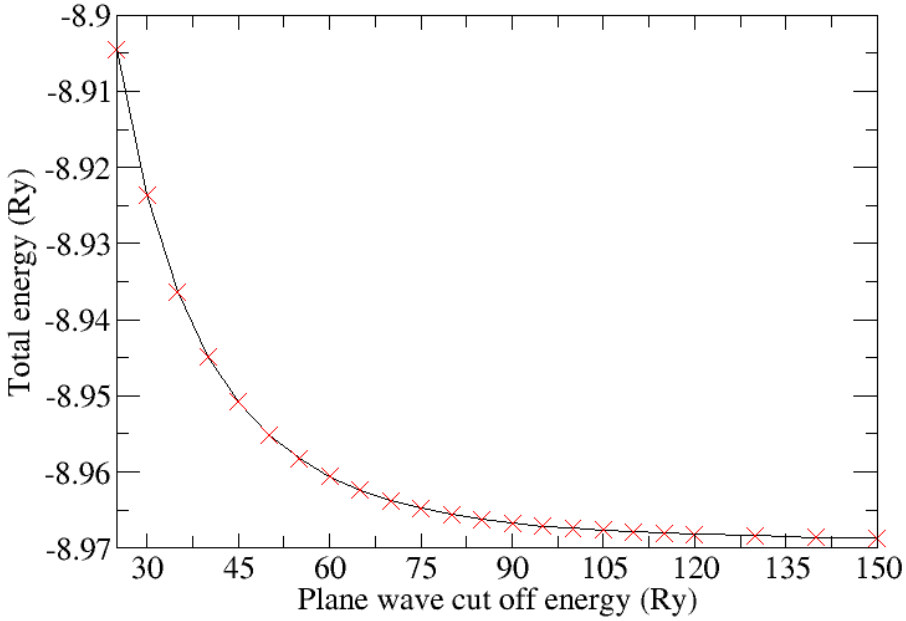

Figure A.4: A plot of the total energy for MgH_2 versus the plane wave cut off energy.

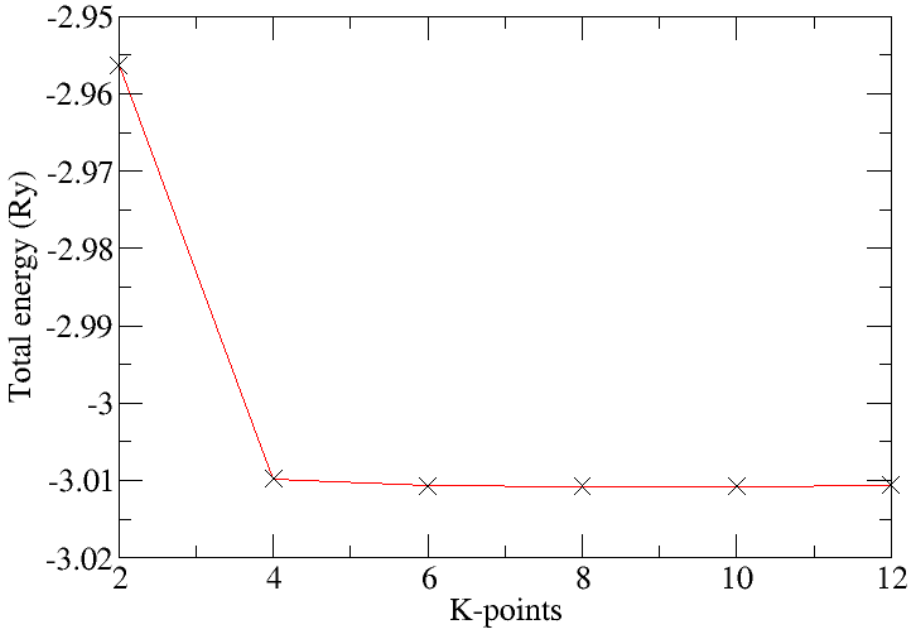

Figure A.5: A plot of the total energy verses k-point mesh for LiH.

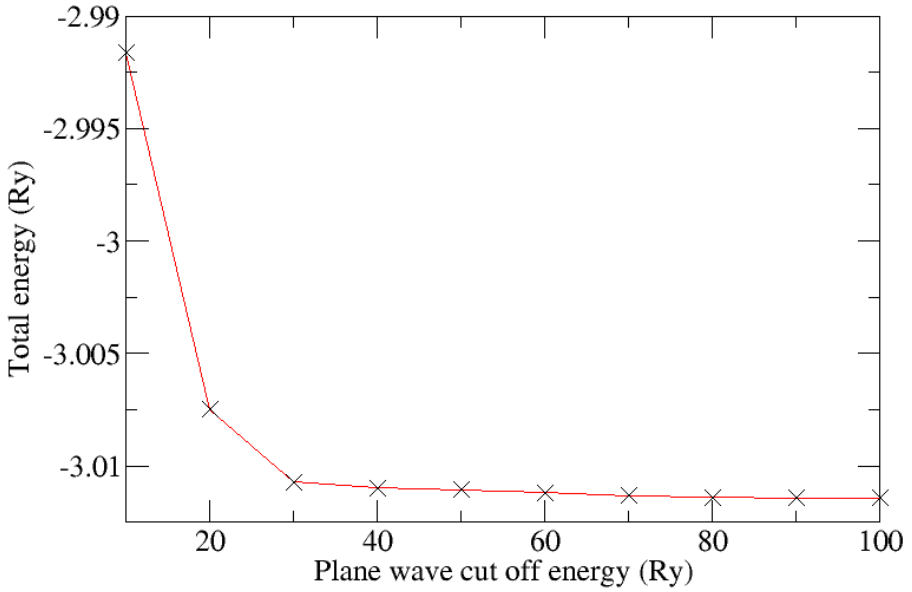

Figure A.6: A plot of the optimized total energy for LiH against the plane wave cut off energy.

APPENDIX B

THERMODYNAMIC PROPERTIES TABLES

Table B.1: Calculated thermodynamic properties for LiH compared with experimental values.

Calculated results					Experimental results [a]	
T(K)	S **(J/mol/K)**	C_v **(J/mol/K)**	**Internal energy**	**Vibrational energy**	S	C_p
0	0.0000	0.0000	0.0000000	0.0000000		
50	0.1939	0.7424	0.0163002	0.0162928		
100	2.0569	5.7997	0.0164136	0.0162570		
150	5.5922	12.0006	0.0167537	0.0161147		
200	9.8388	17.7054	0.0173211	0.0158222		
250	14.3518	22.8267	0.0180950	0.0153620		
300	18.9160	27.2526	0.0190510	0.0147284	20.211	28.089
350	23.4034	30.9444	0.0201615	0.0139221		
400	27.7393	33.9603	0.0213995	0.0129476	29.239	34.795
450	31.8854	36.4032	0.0227411	0.0118116		
500	35.8269	38.3808	0.0241665	0.0105214	37.650	40.737
550	39.5629	39.9878	0.0256600	0.0090851		
600	43.1005	41.3022	0.0272088	0.0075104	45.579	46.378
650	46.4506	42.3853	0.0288031	0.0058045		
700	49.6256	43.2850	0.0304351	0.0039743	53.142	51.876
750	52.6384	44.0383	0.0320984	0.0020264		
800	55.5015	44.6740	0.0337881	-0.0000333	60.424	57.299
850	58.2265	45.2145	0.0355001	-0.0021994		
900	60.8243	45.6771	0.0372312	-0.0044669	67.484	62.678
950	63.3048	46.0759	0.0389786	-0.0068311		
1000	65.6772	46.4216	0.0407402	-0.0092876		

[a](Ihsan, 2006)

Table B.2: Calculated thermodynamic properties of MgH_2 compared with experimental values.

PRESENT WORK					Ref.[a]		Ref.[b]	
T (K)	J mol^{-1} K^{-1}		E_{internal}	$F_{\text{vibration}}$	S	C_{p}	S	C_{p}
	S	C_{v}						
0	0.0000	0.0000	0.0000000	0.0000000				
50	1.4222	4.2697	0.0571520	0.0570300				
100	7.1175	13.3606	0.0578980	0.0566800				
150	13.5072	19.5445	0.0592640	0.0557960				
200	19.5995	24.6945	0.0610870	0.0543770				
250	25.3994	29.5407	0.0633190	0.0524500				
300	30.9707	34.1434	0.0659401	0.0500360	31.01	35.26	31.306	35.499
350	36.3408	38.3965	0.0689262	0.0471540				
400	41.5124	42.2112	0.0722444	0.0438210			42.643	43.283
450	46.4805	45.5573	0.0758571	0.0400540				
500	51.2411	48.4512	0.0797262	0.0358713	53.06	49.99	52.990	49.539
550	55.7939	50.9348	0.0838162	0.0312895				
600	60.1430	53.0594	0.0880953	0.0263268	62.65	55.18	62.528	55.192
650	64.2953	54.8763	0.0925361	0.0210003				
700	68.2598	56.4329	0.0971154	0.0153266	71.49	59.44		
750	72.0466	57.7704	0.1018134	0.0093213				
800	75.6660	58.9240	0.1066137	0.0029991	79.66	62.92		
850	79.1285	59.9230	0.1115023	-0.0036259				
900	82.4444	60.7919	0.1164676	-0.0105411	87.24	65.72		
950	85.6231	61.5511	0.1214997	-0.0177341				
1000	88.6739	62.2171	0.1265903	-0.0251937	94.28	67.95		

[a] (Chase, 1998), [b] (Ihsan, 2006).

APPENDIX C

PSEUDOPOTENTIALS

Pseudopotentials are used to reduce computation time by replacing the full electron system in the coulombic potential by a system only taking explicitly into account the "valence" electrons (that is, the electrons participating in bonding). This approach not only reduces the electron number but also the energy cutoff necessary (this is critical in plane-wave based computations). Computations in this research were performed using the pseudopotentials below:

C.1 Pseudopotentials Used

Mg.pz-n-vbc.UPF

This pseudopotential was used to represent the valence electrons of Mg. It was generated using ld1 code which was authored by Stefano de Gironcoli.

0	Version Number
Mg	Element
NC	Norm - Conserving pseudopotential
T	Nonlinear Core Correction
PZ	Exchange-Correlation functional
2.00000000000	Z valence
0.00000000000	Total energy

Electronic Configuration: $1s^2 2s^2 2p^6 3s^2$

Valence electrons considered: $3s^2 3p^0$

Core electrons: $1s^2 2s^2 2p^6$

nl	**l**	**Occupation**
3S	0	2.00
3P	1	0.00

Li.pz-n-vbc.UPF

This pseudopotential was used to represent the valence electrons of Li. It was Generated using ld1 code, authored by P. Giannozzi.

0	Version Number
Li	Element
NC	Norm - Conserving pseudopotential
T	Nonlinear Core Correction
PZ	Exchange-Correlation functional
1.00000000000	Z valence
0.00000000000	Total energy

Electronic Configuration: $1s^2 2s^1$

Valence electrons considered: $2s^1 2p^0$

Core electrons: $1s^2$

nl	**l**	**Occupation**
2S	0	1.00
2P	1	0.00

H.pz-vbc.UPF

This pseudopotential was used to represent the valence electrons of H. It was generated using ld1 code which was authored by P. Giannozzi.

0	Version Number
H	Element
NC	Norm - Conserving pseudopotential
F	Nonlinear Core Correction
PZ	Exchange-Correlation functional
1.00000000000	Z valence
0.00000000000	Total energy

Electronic Configuration: $1s^1$

Valence electrons considered: $1s^1$

Core electrons: $1s^1$

nl	l	Occupation
1S	0	1.00

C.2 Pseudopotentials Choice

Mg.pz-n-vbc.UPF

The pseudopotential for Mg was chosen because it had already provided accurate and reliable results in other works as used by the authors in the following papers:

1. Surface oscillatory thermal expansion: Mg (10-10), Ismail, E.W. Plummer, M. Lazzeri, and S. de Gironcoli, Phys. Rev. B 63, 233401 (2001).

2. First principles thermoelasticity of $MgSiO_3$-perovskite: consequences for the inferred properties of the lower mantle, B.B. Karki, R.M. Wentzcovitch, S. de Gironcoli, and S. Baroni, Geophys. Res. Lett. 28, 2699 (2001).

3. High pressure lattice dynamics and thermoelasticity of MgO, B.B. Karki, R.M. Wentzcovitch, S. de Gironcoli, and S. Baroni, Phys. Rev. B 61, 8793 (2000).

4. Ab-initio lattice dynamics of $MgSiO_3$ perovskite at high pressure, B.B. Karki, R.M. Wentzcovitch, S. de Gironcoli, and S. Baroni, Phys. Rev. B 62, 14750 (2000).

5. Effects of short-range-order on the optical properties of the $Zn_xMg_{(1-x)}S_ySe_{(1-y)}$ quaternary alloy, A.M. Saitta, S. de Gironcoli, and S. Baroni, Appl. Phys. Lett. 75, 2746 (1999).

6. First-Principles Determination of Elastic Anisotropy and Wave Velocities of MgO at Lower Mantle Conditions, B.B. Karki, R.M. Wentzcovitch, S. de Gironcoli, and S. Baroni, Science 286, 1705 (1999).

7. Structural and Electronic Properties of a Wide-Gap Quaternary Solid Solution: (Zn, Mg)(S, Se), A.M. Saitta, S. de Gironcoli, and S. Baroni, Phys. Rev. Lett. 80, 4939 (1998).

H.pz-vbc.UPF

The choice of the pseudopotential for Hydrogen relied to a much extent on the choice of the Mg pseudopotential. This is because there is a wide choice of pseudopotentials for hydrogen unlike the case of Mg whereby the choice of the pseudopotentials was limited. In the DFT calculations, the pseudopotentials for a compound must be similar in terms of the exchange correlational functional and the author otherwise the calculation would fail. This reason led to the choice of this pseudopotential because a Norm Conserving pseudopotential that was authored by Perdew and Zunger was required to be used together with the Mg pseudopotential.

APPENDIX D

CONFERENCE PRESENTATIONS AND SCHOOLS ATTENDED

D.1 Conference Papers

1. Magero Denis, Makau Nicholas, Amolo George and Lusweti Kituyi. *Ab-initio* studies of lithium hydride and magnesium hydride for hydrogen storage applications. The Nanotechnology and Materials Science Conference, Kenyatta University, 18^{th} to 20^{th} July, 2012.

2. Magero Denis, Makau Nicholas, Amolo George and Lusweti Kituyi. Materials for the hydrogen storage economy: Lithium hydride and magnesium hydride. The 2^{nd} Science, Technology and Innovation week organized by the National Commission for Science, technology and innovation, Kenyatta International Conference Centre (K.I.C.C) Nairobi, 13^{th} to 17^{th} May , 2013.

D.2 Schools Attended

1. Quantum Espresso and Quantum Monte Carlo Workshop. Chepkoilel University College (Moi University), KENYA, 6^{th} March, 2012 to 8^{th} March, 2012.

2. The 2^{nd} African School on Electronic Structure Methods and Applications (ASESMA 2012). Chepkoilel University College (Moi University), KENYA, 28^{th} May to 8^{th} June, 2012.

3. School on Numerical Methods for Materials Science Related to Renewable Energy Applications. International Centre for Theoretical Physics, Trieste, ITALY, 26^{th} to 30^{th} November, 2012.